6

Mechanical Properties of Human Mineralized Connective Tissues

R. De Santis, L. Ambrosio,

IMCB Institute for Composite and Biomedical Materials
National Research Council
I-80125 Napoli, Italy

F. Mollica,

University of Ferrara
Department of Engineering
I-44100 Ferrara, Italy

P. Netti, and L. Nicolais

University of Naples "Federico II"
Department of Materials and Production Engineering
I-80125 Napoli, Italy

Abstract. Experimental work has to be tightly linked with modeling. In fact, successful modeling requires firstly comparison with experiments in order to verify its predictions or to set its range of validity. Secondly, experiments measuring the mechanical properties of tissues are needed as input to calibrate mechanical models of organs that can be used to run simulations *in silico*. In this chapter we wish to provide a comprehensive

literature review covering the mechanical characterization of hard tissues, in particular compact bone, trabecular bone and dentine.

Elastic and strength properties of such tissues are carefully reviewed, together with fracture mechanics properties when available. Properties obtained from different measurement devices are gathered and compared with each other. The anisotropy and the inelasticity of the mechanical properties of hard tissues is particularly stressed.

6.1 Introduction

Over the past half century, research on the evaluation of the mechanical properties of mineralized connective tissues (hard tissues) has been extremely active. It remains predominantly a fundamental research field, motivated by two principal objectives. The first is to achieve a deeper knowledge of the relation between the tissue structure and the mechanical properties in order to develop diagnostic tools. The second is to improve the design of prosthetic devices used as hard tissue substitutes.

The reliability and the significance of mechanical measurements upon hard tissues are dependent on a wide range of factors. These include anisotropy, time-dependent properties (e.g. viscoelasticity), the patient's sex and age, the organ from which the specimen is taken, its site and its adaptation, and response to the loads, diseases, or traumas experienced. Also, specimen conditioning (e.g. storage conditions and temperature) has a major influence upon mechanical properties. The difficulty in obtaining specimens of suitable dimensions for testing is also a significant issue.

6.1.1 Mechanical Testing

Mechanical properties have been assessed through several direct and indirect measurements of stress and strain.

Testing using dynamometers is the basic direct method for estimating the mechanical properties of tissue specimens loaded in tension, compression, bending, shear, or torsion. A dynamometer consists of an actuator mounted on a frame. Loading cells and displacement sensors are used to measure the load and the deformation, respectively. This analysis can be carried out in static or dynamic conditions thus providing direct information on the static, viscoelastic, and fatigue behavior of materials. This investigation technique has been widely performed on macroscopic and microscopic specimens, the latter having cross-sectional areas of a few

square millimeters. This essentially characterizes standard mechanical and micromechanical testing [ERa, DOa].

Ultrasonic testing provides information on the elastic properties of materials by measuring the longitudinal and shear speeds of sonic waves propagating into the material. The equipment used principally comprises a piezoelectric transducer and a sensor. Although this technique does not provide mechanical strength information, it is especially useful in order to detect the anisotropy of materials by determining the elastic constants. In fact, compared to classical mechanical testing, it is not destructive, thus the same specimen can be used for further analysis in different directions. Moreover, ultrasonic testing—which measures resonant frequencies, rather than wave speed—allows the assessment of mechanical anisotropy from one measurement at a single orientation of the specimen. A further advantage of ultrasonic testing is its tolerance of a diversity of specimen geometry and size. Specimen shapes need not be particularly refined, and very small specimens may be tested [SKa].

Indentation testing has mainly been used to measure the hardness of materials, from which the Young's modulus can be derived. An indenter is applied to the specimen, whose hardness is calculated by measuring the load and penetration depth. Compared to the mechanical investigation techniques outlined earlier, testing with an indenter provides data indicative of surface properties rather than bulk properties. This method is particularly attractive for the simplicity of the equipment, and also because it enables the mapping of properties as a function of the site. This technique has further evolved over recent decades with the emergence of mechanical analysis by atomic force microscopy (AFM). This basically consists of using an indenter tip, with dimensions of the order of a few atoms, and a laser to detect the interference between the tip and the substrate material. With AFM, it is possible to identify variation in local hardness at a nanoscale level [LAb, CHa]. Scanning acoustic microscopy (SAM) is a very promising tool for nondestructive investigations of the elastic properties of a material at a scale resolution level similar to optical microscopy. The image contrast and fringes are related to both superficial and bulk elastic properties of the material [YUa, KAb].

In the last two decades fracture mechanics testing has been used to evaluate the fracture toughness of hard tissues by applying linear elastic fracture mechanics (LEFM). Fracture toughness plays a decisive role in hard tissue functionality by determining the level to which the material can be stressed in the presence of cracks, or, equivalently, the magnitude of cracking that can be tolerated at a given stress level. The major effort has concentrated on propagation of the crack using a variety of precracked specimens: three-point bending specimens, compact tension specimens (CT), single edge-notched specimens (SEN), center-notched cylindrical specimens

(CNC) and compact sandwich specimens. The CT geometry has proved to be the most useful for studying Mode I fracture mechanics of hard tissues [DOa, DEb].

6.1.2 Imaging

Mechanical properties of hard tissues are strongly related to the structural organization of the constituent materials. Optical or light microscopy is the first technique used to analyze small objects, their images being magnified through convex lenses, and the polarizing microscope is largely used for the examination of thin sections of materials. A method of particular value in examining living tissues is phase-contrast microscopy, which detects the phase differences due to the variations in the refractive index of material structures by imaging light intensity variations.

Through electron microscopy, sharper images, which better distinguish the hierarchical organization of living tissues, are observed below the resolution level of the optical microscopy with a greater depth of focus. This technique detects the interactions between an electron beam and the material. Images are formed either directly, by focusing the electron beam that passes through a thin specimen (transmission electron microscopy, TEM), or indirectly by using the information carried by secondary electrons or X-rays (scanning electron microscopy, SEM). Specimens are often coated with heavy metals. Environmental SEM has recently been developed. This has the advantage of eliminating artifacts due to the staining process, which modify the structure. Moreover, this imaging technique is particularly attractive for living tissues, because the hydrated state of the specimen can be preserved [BOd, BRa]. Topographic imaging of hard tissue at a very low resolution may also be obtained using AFM and SAM [LAb, CHa].

The X-ray computed microtomography (X-ray μCT) is a 3-D microscopic technique developed over the past 20 years and it is a miniaturized version of the well-known computer axial tomography method used for medical imaging. This new method of microimage analysis has gained attention in experimental biomechanics due to its ability to measure accurately the mineral content of tissues. The result of the X-ray μCT is in the form of a three-dimensional image reconstructed on the basis of multisliced planar tomographs taken at a fine angular pitch along the rotational axis. Moreover, compared to the previous microscopy techniques, the 3-D structure organization of specimens is detected in a nondestructive manner [WEb, DEa].

6.1.3 Structure–Property Relationship

Attaining knowledge of the relationship of the structure of living hard tissue to the physical and mechanical properties it exhibits is one of the principal

objectives of this field of research. Along with this, the characterization of interfaces, such as those of synthetic devices with biological tissues, is a topic of extreme importance. For instance, a sufficiently precise identification of the structure–property relationships could facilitate diagnosis in certain clinical conditions. Unfortunately, as of today, the available data are rather poor but more refined structure–property correlations towards increasing levels of precision are an actual research target. In particular, structural correlations are sought with macroscopic quantities that are easily measurable. The measurement of tissue density probably represents the first notable attempt adopting this strategy. However, this quantity is not completely satisfactory because, at a macroscopic level, density alone is not adequate to distinguish tissue anisotropy. The investigation of the constituent materials' organization and distribution within the tissue therefore remains a compelling need. As a model is defined, its calibration passes through in vitro and in vivo testing. The main function of a hard tissue is to sustain and transmit loads, therefore mechanical testing is extremely important in order to validate mechanical models. Accordingly, density and microstructural organization information—obtained from microcomputed tomography imaging—combined with homogenization methods and finite element modeling (FEM), can be extremely useful to determine the material properties of a tissue. Thus the potential of all these methods, when used in a combined way, to characterize the mechanical behavior of the tissue and relate this to the disease state suggests great promise for its use in clinical diagnostic investigations [HOa, NIc].

In the following sections, the mechanical properties of human hard tissues—such as trabecular bone, compact bone, and dentine—are reviewed. Particular emphasis is placed upon the measurement of tissue anisotropy.

6.1.4 Hierarchical Structures in Hard Tissue

Figure 6.1 presents the hierarchical structure of a hard tissue related to imaging and to mechanical characterization methods and capabilities.

The main constituents of hard tissues are the extracellular matrix (i.e. collagen, apatite, and water), which mainly provides mechanical support, and cells (viz. osteocytes in bone and odontoblast in dentine) which, among various tasks, continuously control and adapt the extracellular matrix with the aim of achieving an optimal performance. It is considered that the mechanosensitivity of cells is related to the processes intimately connected with the mechanical behavior of the extracellular matrix [YOa] The extracellular matrix of bone consists of the soft and ductile collagen fibrils, reinforced by the stiff and brittle apatite crystals. Water is located within the fibrils and within the triple-helical molecules at a subnanostructure level. The collagen fibrils—about 100 nm in diameter—are held together

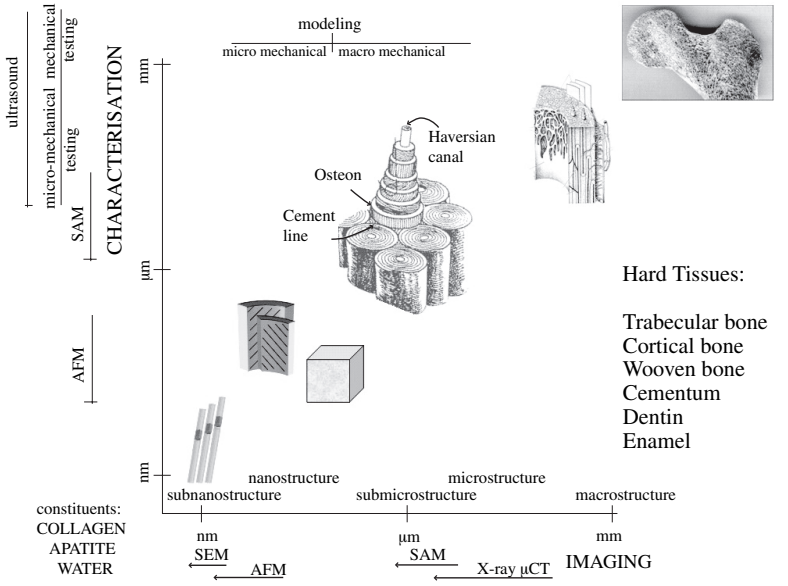

Figure 6.1. Hierarchical structure of hard tissues and characterization capabilities of mechanical and imaging techniques.

by a nonfibrillar organic matrix that acts as a glue. Less than 1% by weight of this glue would be enough to provide a link between the mineralized fibrils adequate to confer the known toughness properties to bone [THa, CUc, FAb]. Because the elastic properties of collagen and hydroxyapatite are about 1.5 GPa and 110 GPa, respectively, this is the range of stiffness one has to expect for hard tissues. Indeed, in the human body, enamel, basically constituted by apatite prismatic crystals, is the stiffest hard tissue, showing a Young's modulus of about 100 GPa. On the other hand, spongy (or trabecular) bone presents the lowest Young's modulus values. However, trabecular bone is a porous material and experimental values of elastic modulus have to be interpreted as apparent values. In fact, true trabecular tissue properties suggest an elastic modulus between 10 GPa and 20 GPa [WEa, ZId, SIa].

6.1.5 Elastic Properties of Individual Trabeculae

A notable account of the mechanical properties of individual trabeculae is already available [KEa]. Early investigations focused on direct measurements, obtained through buckling and bending tests on individual trabeculae. These reported mean elastic modulus values of 8.69 GPa [RUa]

and 7.8 GPa [MEa]. More recently, through microtensile tests on long, uniform, rodlike trabeculae from human tibia, a mean value in tension of 10.4 GPa has been published. In contrast, ultrasonic measurements of similar individual trabeculae suggest an elastic modulus of 14.8 GPa [RHa].

Differences between direct mechanical testing and the wave propagation techniques are partially related to artifacts that affect direct mechanical measurements. Moreover, bone is a viscoelastic material, therefore strain rate dependence of the measured properties is to be expected. In general, the elastic modulus is an increasing function of strain rate. Consequently, continuous wave experiments give higher values of the elastic modulus because the strain rate is much higher than those performed by traditional dynamometers.

Higher values of the Young's modulus are recorded using the AFM nanoindentation technique. Individual trabeculae from the proximal femur are found to be significantly subject-dependent. The elastic modulus range is between 6.9 and 15.9 GPa, with an average value of 11.4 GPa [ZYa]. Elsewhere, the elastic modulus derived from nanoindentation of individual trabeculae from lumbar vertebrae is estimated to be 19.4 GPa [RHa].

In addition, SAM investigations have also been carried out on individual trabeculae from lumbar vertebrae. An average elastic modulus of 7.47 GPa is obtained for trabeculae from young individuals. This value decreases by about 30% for middle-aged and older people [ZHa]. Using trabecular material from the distal femur, a higher Young's modulus value (17.50 GPa) can be derived from SAM. Consistency with AFM investigations is also observed [TUa]. Similar average values of the Young's modulus obtained through SAM are later reported [BUa].

It is interesting to note that experimental results on individual trabeculae and single osteons, obtained in the same testing condition, generally provide higher values for the Young's modulus of osteons. Therefore, studies focusing on the mechanical properties of bone material at a microscale level divide into two groups. The first one assumes that trabeculae and osteons can be treated in the same manner, whereas the second one distinguishes trabeculae from osteons, on the basis of their different mechanical properties.

6.1.6 Elastic Properties of Single Osteons

The mechanical behavior of a single osteon is an intriguing research field, its study providing structural insights at both the macro and nano level. In fact, given the properties of a single osteon, the mechanical performance of a whole bone could be obtained and this can be useful also to validate averaging models against mechanical properties measured in a traditional way.

The effects of lamellar orientation on the tensile properties of single osteons were observed long ago. Osteons whose lamellae are mainly oriented in the longitudinal direction (dark osteons) are characterized by an elastic modulus of 12 GPa and a strength of 120 MPa, and an elastic modulus of 5.5 GPa and a strength of 102 MPa is found for osteons with lamellae oriented in intermediate directions [ASc]. The same authors later recorded a lower stiffness in compression [ASb] becoming even lower in bending [ASa]. The confidence in the strength values reported here is merited, because the load is constant in each cross-section during testing. The same, though, does not hold for strain, whose measurement is affected by the dynamometer compliance, thus leading to systematic errors in the measurement of the elastic modulus. Recently, nanoindentation tests in the longitudinal direction of cortical tibia provided elastic modulus values of 22.4 GPa and 25.7 GPa for the osteon and the interstitial lamellae, respectively [ROb].

Similar values have been measured in lamellae of dry cortical bone from the femoral neck; moreover, using low depth indents, thick lamellae results in stiffer rather than thin lamellae, therefore suggesting a longitudinal orientation of mineralized fibers in thick lamellae [HEa]. Comparable AFM indentation results have been obtained on the cortical bone from the femoral mid-shaft, the reported values being 24.36 GPa and 20.34 GPa for thick and thin lamellae, respectively [XUb]. However, it is important to notice that indentation measurements on cortical bone depend on the indentation depth, on the environmental conditions, and specimen preparation [HEa, XUb]. Moreover, the indentation modulus is determined somehow arbitrarily, that is, by assuming a certain value for the Poisson ratio. It is notewnorthy, however, that SAM investigation of cortical bone from the proximal femur also suggests a difference of about 20% between the acoustic impedance of lamellae with high and low reflectivity (thick and thin lamellae, respectively). The highest impedance values are obtained for the innermost lamellae, whereas the mean impedance of secondary osteons is higher than primary osteons [RAb]. The outermost lamellae of osteons are always more compliant [BUa] and the average elastic modulus derived from SAM investigations on cortical bone from the mid-shaft of the femur in the longitudinal and transverse directions are 20.55 GPa and 14.91 GPa, respectively [TUa].

A strong correlation between crystal features (essentially, shape and size) and the mechanical properties of osteons would be expected, though. Bone is more brittle in older and osteoporotic animals, where large size crystals are observed, whereas it is stronger and tougher in young animals, where a broader crystal size distribution is reported. Crystal size increases in osteoporotic and in aging bones [BOc]. Through X-ray investigations, structure distortions pictured as orientation of crystals have been observed in both longitudinal and alternate osteons cyclically loaded at a

high stress level. Higher distortions are detected for longitudinal osteons. This supports the hypothesis that this type of osteon is more prone to buckling, and suggests that the thicker crystallites that are between the collagen fibers are more easily unbound from the matrix as a consequence of buckling [ASd].

The elastic behavior of osteons has also been predicted by several composite models. Common inputs are the elastic modulus of collagen (range 1.0 GPa to 1.5 GPa), the elastic modulus of apatite crystals (range 110 GPa to 150 GPa), and the Poisson ratio of 0.3. The analysis of the mechanical response of composite materials involves investigations on the micro- and macroscale level [NIc]. Using a cross-ply model of the osteon and an homogenization procedure for the properties of lamellae, a value of the elastic modulus of 22 GPa in the longitudinal direction is obtained at a mineral concentration of 0.6 [LEa]. However, the same concentration leads to very low values in the transverse direction. Incorporating the three partial porosities of bone [COc] related to Haversian canals, Volkman's canaliculi and lacunae, the typical elastic orthotropic constants of bone are derived using an hydroxyapatite content of 35% and an overall porosity of 8% [SEa]. Instead, modeling at the submicrostructural level the single lamella and using routines developed for a random network of cellulose fibers, nonuniform strains and clustering of aligned fibrils are displayed under load simulations [JAb]. However, model results of compact bone are still misleading because there are no reliable data regarding the properties of the constituent materials and interfaces [RHb]; moreover, at the macroscale level, the nondestructive imaging of the structure through micro-CT is not as powerful as it revealed to be for trabecular bone.

6.2 Trabecular Bone

Trabecular, cancellous, or spongy bone is abundant in the inner regions of the epiphysis of long bones, in the mandibular bone, within vertebral bones, and in flat and irregular bones. Therefore, this material represents the core of bony organs. The constituent materials are collagen, apatite, and marrow, differently organized across sites according to the specific adaptation process. The trabeculae are organized in very complex networks, which constitute an open porosity occupied by the bone marrow. The similarity between these organizations and engineering foam materials classifies trabecular bone within cellular solids, whose microstructural features affect the mechanical behavior. The microscopic level of the hierarchical organization of trabecular bone distinguishes rods and plates as the basic elements of the cellular structure.

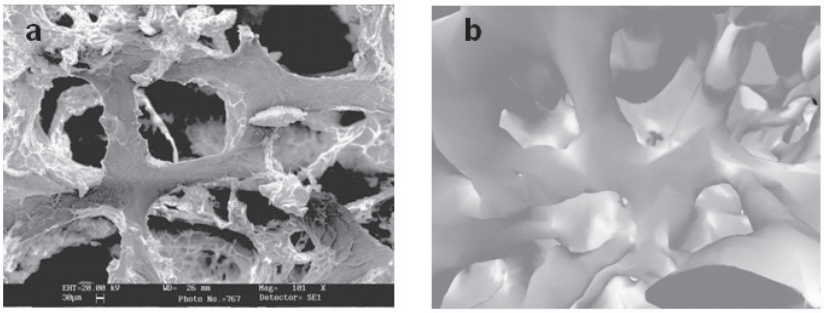

Figure 6.2. Trabecular bone network of a 50-year-old man: (a) SEM image (courtesy of Prof. D. Ronca, Orthopedic Clinic, II University of Naples, Italy); (b) 3-D reconstruction of micro X-ray CT (courtesy of Prof. S. Rengo, School of Dentistry, University of Naples Federico II, Naples, Italy).

6.2.1 Tibial Trabecular Bone

Trabecular bone obtained from human tibia has been used extensively, because this tissue is very abundant in the proximal tibial epiphysis thus providing the possibility to fabricate macroscopic specimens used for standard mechanical testing. Moreover, the proximal tibial epiphysis is important because of the prosthesis that is often required to alleviate certain pathologies of the knee. Figures 6.2a and b show the structural organization of trabeculae inside the subchondral trabecular bone of a 50-year-old man, depicted through SEM and X-Ray μCT, respectively.

This tissue is obtained from the weight-bearing area of proximal tibia, as depicted in Figure 6.3. A different mechanical behavior has been commonly observed between the medial and the lateral condyle region, and a strong anisotropy is generally recognized [KEb]. The relationship between trabecular orientation and mechanical properties in the longitudinal direction of the tibia (direction 3 of Figure 6.3) has been a matter of concern since about 1980. A complete map of the Young's modulus in this direction (E_3) related to the subchondral bone plate shows a marked site dependency [GOa]; in agreement with biomechanical models of femur–knee–tibia, the medial region is stiffer than the lateral region. A maximum peak value of 433 MPa is distinguished in the medial region. The mechanical method employed is the compression test on cylinders of 7 mm $\times$ 10 mm. A more precise average value of E_3 is later obtained by using compression and tension tests and measuring local deformations through an extensometer with 20-mm gauge length; mean values of 485 MPa and 483 MPa measured in compression and tension, respectively, have been obtained suggesting no statistical difference in the Young's modulus along direction 3 according

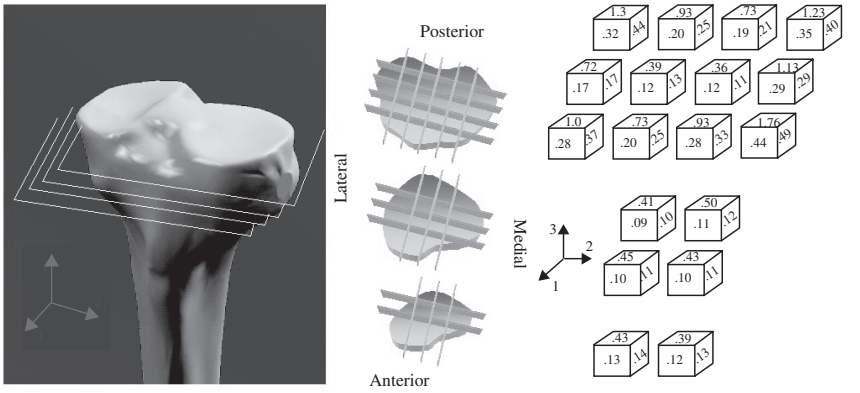

Figure 6.3. 3-D reconstruction of proximal tibia. Anisotropy in the Young's modulus of trabecular bone [RHd]. Values are expressed in GPa.

to the mode of loading [ROa]. More recently, optimized protocols for machining macroscopic specimens, obtained from the medial and the lateral regions, have been used. These employ 5-mm gauge length extensometers, thus preventing edge effects of previous investigations. In this case average values of $E_3 = 1091$ MPa (S.D.634) and $E_3 = 1068$ MPa (S.D.840) have been obtained in compression and tension, respectively [MOa]. Compression measurements of E_3 generally reveal that trabecular bone is stiffer in the medial condyle than in the lateral condyle region [GOa, DIa].

It is evident that a strong variation of E_3 according to the site is to be found also along the longitudinal direction. On the other hand, by using the ultrasonic investigation technique and smaller specimens, the Young's modulus anisotropy of trabecular bone has been measured through a complete 3-D mapping of the tibial epiphysis [RHd] as depicted in Figure 6.3. Also, these findings are in qualitative agreement with earlier measurements through penetration tests [HVa].

Unfortunately, the agreement among material properties measured using a variety of equipment setups, specimen geometry, environment, and mechanical conditioning is in the best cases qualitative rather than quantitative. If data obtained in tension, compression, and bending of trabecular bone from a specific site of the tibia are compared, an inconsistency of the results is generally observed. The statistical difference becomes more evident as the set of mechanical data includes micromechanical tests. In particular, a value of the Young's modulus of 4.59 GPa is obtained through microbending tests [CHb], whereas microtensile and ultrasonic tests on individual dry trabeculae provide an elastic modulus of 10.4 GPa and 14.8 GPa, respectively [RHa]. In contrast, the Young's moduli derived from

nanoindentation tests on trabecular bone are estimated to be 19.6 GPa and 15.0 GPa in the longitudinal and transverse directions, respectively [RHb], thus in a range similar to that of compact bone. It is clear, then, that the Young's modulus of trabecular bone is strongly dependent on the specimen dimensions. Macroscopic specimens can be regarded as a porous structure delimited by a trabecular network. Accordingly, mechanical measurements need to take into account the effective volume fraction of bone. Indeed, bone density is the parameter most commonly used to determine the variations of the Young's modulus, which is assumed to depend on density through a power law. However, the precise form of this relationship and the fact that the modulus would be a function of density alone is controversial: the trabecular architecture is known to play a crucial role in the properties of the material [KEb] and density cannot take this into account. Instead, mechanical testing on microscopic specimens (i.e. individual trabeculae) and nanoindentation measurements provide the true elastic modulus of bone, which indeed produces results very close to the value measured for compact bone. Efforts to account for the structural anisotropy of trabecular bone are described by a general theory relating the elasticity tensor to the fabric tensor [COd, COb]. Age-dependence variations in the Young's modulus are generally described by a nonlinear relationship: this property increases up to about 45 years and significantly decreases after 60 years [DIa].

As with the Young's modulus, the strength of trabecular bone also depends on the loading direction, the site, and the age. The strength is higher in the longitudinal direction, and tension measurements provide yield stress values lower than in compression [MOa]. The trabecular bone strength can vary by an order of magnitude across the tibia sites, spanning between 1 and 10 MPa, and the medial subchondral bone region appears to be tougher than the lateral region [DIa]. A power law relation between strength and density is generally observed [KEb]. Again, this relationship is controversial because the trabecular architecture plays a fundamental role in determining bone strength. The strength dependence on age follows a similar trend observed for the Young's modulus. Table 6.1 presents the yield and the ultimate stresses and strains of trabecular bone from the tibia, depending on age [MOa, DIa].

6.2.2 Trabecular Bone from the Vertebral Body

The vertebral body is another site from where trabecular bone tissue is often harvested in order to determine its mechanical properties. This tissue is particularly abundant in the vertebrae from the lumbar region of the spine. The knowledge of the mechanical behavior of trabecular bone from this site of the body is particularly important because of various pathologies that

Age(Years)	16–39	40–59	60–83
Compression			
Ultimate Stress [MPa]	10.6	9.86	7.27
Ultimate Strain [mm/mm]	2.48 %	2.12 %	2.05 %
Yield Stress [MPa]		5.83	
Yield Strain [mm/mm]		0.73 %	
Tension			
Yield Stress [MPa]		4.50	
Yield Strain [mm/mm]		0.65 %	

Table 6.1. Yield, ultimate stresses, and strains of trabecular bone from tibia.

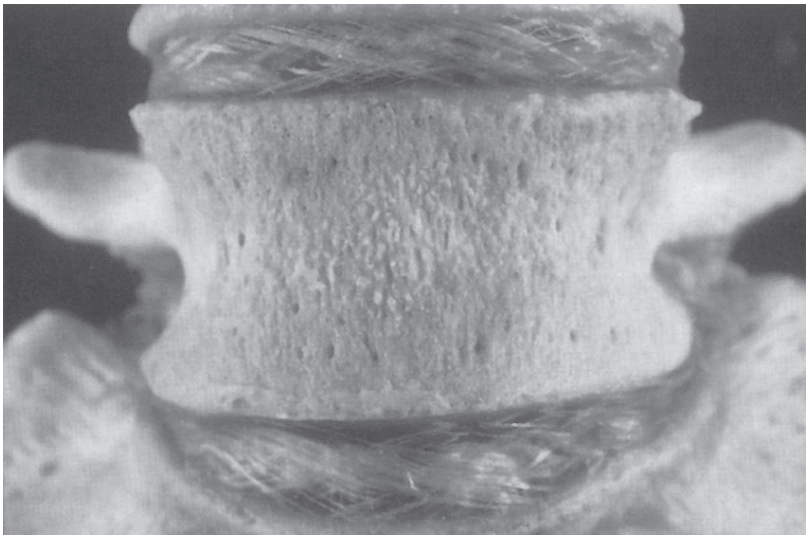

Figure 6.4. Optical image of a vertebra and the intervertebral discs. A main pattern of trabeculae orientation along the longitudinal axis is evident.

can affect the vertebral bodies, such as osteoporosis. Another important point is that the prosthetic devices that are often required to solve a spinal injury or disease will be in contact with this tissue.

Figure 6.4 shows an optical image of a vertebra; the intervertebral disc fibers are also shown. A main pattern of trabeculae orientation along the longitudinal axis is evident.

Figure 6.5 shows the 3-D image of a lumbar vertebra. The bone's image along a coronal section from an L3 vertebra of a 35-year-old man is provided. A trabecular network, principally oriented along the longitudinal direction, is rendered clearly visible through optical microscopy.

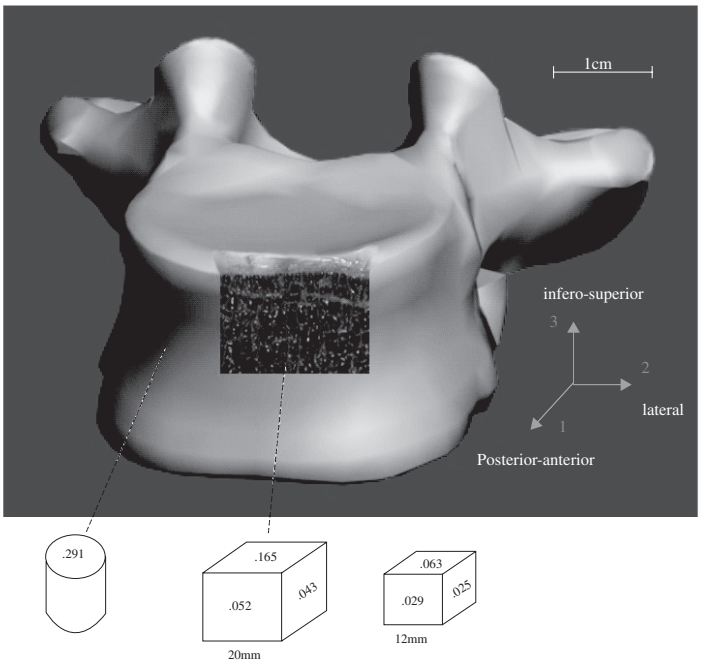

Figure 6.5. 3-D imaging of a lumbar vertebra showing Young's modulus anisotropy and site dependence. Values are expressed in GPa [NIb, AUa].

Compression, bending, and torsion are the loads that act on the spine through complex articulations between vertebrae and intervertebral discs [CAd, CAe]. The orientation of trabeculae along the axes of the spine suggests the adaptation to a compressive stress field transmitted through each vertebra. Trabeculae align along the direction of the functional principal stresses, as hypothesized by Wolff's law [WOa, COe, HUa].

Uniaxial compression tests on vertebral trabecular bone along the cephalo-caudal or superior–inferior direction (direction 3 of Figure 6.5) have been approached using cylindrical and cubic specimens. This direction is perpendicular to the articular end-plates [CAe] and the related properties are thus expected to be higher than those measured in the other directions. A mean value of 67 MPa for the elastic modulus of bone from the central part of the first lumbar vertebra in 15–87-year-old individuals has been measured [KEb, MOb]. Later, investigations in compression and in tension on bone specimens of 8-mm diameter, obtained from the lateral regions of thoracic and lumbar vertebrae, produced mean values of 291 MPa and 301 MPa, respectively [KOb]. Data reprocessed by using a 5-mm

gauge length extensometer implied compression and tension mean values of 344 MPa and 349 MPa, respectively [MOa].

As with bone from the tibia, a marked anisotropy is also observed for vertebral trabecular bone.

Figure 6.5 reports the elastic modulus, determined in compression on cubic specimens from lumbar vertebrae, according to the posterior–anterior, the lateral, and inferior–superior directions (direction 1, 2, and 3, respectively, of Figure 6.5). Again, a variation between results obtained on cubic specimens with sides 20 mm [NIb] and 12 mm [AUa] is clearly evident. Not only do the mean values differ, but also the anisotropy—that is, the ratio between the modulus in the principal direction and the modulus along the orthogonal direction—is different. This inconsistency is due to the mechanical set-up and to bone quality. Furthermore, specimen conditioning can have a marked effect on the mechanical properties. In these studies, the specimens of 20-mm length were stored frozen at $-20°C$, while those of 12-mm length were kept in a saline solution at $4°C$. The site from where the tissue is harvested is also of significance.

As expected, the Young's modulus determined through ultrasonic tests gives significantly higher values of the elastic modulus. The wave speed measurements are mainly related to the trabecular struts, and the mechanical sound signal is faster than the strain rates induced with dynamometers. A mean value of 9.98 GPa is derived from ultrasonic tests [NIb] whereas the mechanical anisotropy is described by speed values of 1545 m/s, 1540 m/s, and 1979 m/s in directions 1, 2, and 3, respectively, in Figure 6.5 [NIa]. It is important to observe that mechanical compression studies on bone anisotropy generally use a single specimen to detect the property for all three loading directions. Therefore, using a low strain level, it is assumed that the material behavior is not affected by previous mechanical tests. However, measurements of the elastic modulus through destructive tests performed after the investigation at low strain levels suggest an increase of the modulus of about 25% [AUa].

In contrast, local measurements using the nanoindentation technique provide higher values of the elastic modulus. An advantage here is that the data can be directly related to specific areas of the trabecular material. The derived Young's moduli obtained on specimens with a thickness of 3 mm from the mid-sagittal plane of the L1 vertebra are 19.4 GPa and 15.0 GPa in the longitudinal and transverse directions, respectively [RHc]. Surprisingly, a detailed map of the elastic properties suggests that the material is stiffer in the transverse, rather than the longitudinal, direction. Measurements taken at a microstructural level also reflect the local variation in the extent of mineralization [ROb].

Table 6.2 summarizes the mechanical properties derived from destructive tests.

Method	Y. Stress (MPa)	Y. Strain (mm/mm)	U. Stress (MPa)	U. Strain (mm/mm)	Ref.
Compression	1.92	0.84 %	2.23	1.45 %	Kopperdahl, Keaveny, 98
Tension	1.75	0.78 %	2.23	1.59 %	
Compression	2.02	0.77 %			Morgan, Keaveny 01
Tension	1.72	0.70 %			
Compression			1.3	2.9 %	Augat et al. 98

Table 6.2. Ultimate properties of trabecular bone from vertebra.

6.2.3 Trabecular Bone from the Femur

The femoral head is one of the sites where the mechanical properties of trabecular bone are of great importance. Bone fractures at this location are a common injury especially in old people. The hip joint bears and transmits very high loads, amplified by the offset between the acetabular axis and the femoral axis. Several investigations focus on the mechanical properties of this bone, in order to improve preventive, therapeutic, and prosthetic strategies. Very complex patterns of stress distribution in the whole femoral proximal epiphyses and its single head are documented [VAc, APa].

Compression tests, using 12 mm in diameter cylindrical specimens, give the difference in the elastic moduli values in the anterior–posterior direction for inferior and superior sites on the head (Figure 6.6). As indicated by radiographs of healthy and osteoporotic femoral heads [VAc], a higher porosity is found in the inferior region, where the compressive modulus is five times lower. Surprisingly, no statistical differences are observed between the elastic properties of normal and osteoarthritic bones [BRb].

Compression tests on 8-mm cubic specimens from the region immediately inferior to the epiphyseal line, oriented along the superior–inferior direction (the primary compressive axis) provide a higher value of the elastic modulus (Figure 6.6). Again, no difference is observed in the modulus between tissues from cadavers and fractured hips [CIa, HOb]. It is clear from these results that the elastic modulus depends on the region and direction of loading and the strong mechanical anisotropy is already well evident. The elastic modulus of macroscopic trabecular specimens reaches values up to 1 GPa [CIa].

The elastic modulus measurements, averaged in the whole proximal femur, suggest values of 0.13 GPa, 0.06 GPa, and 0.05 GPa in the axial, sagittal, and coronal direction, respectively [AUa, MAa], thus indicating a certain degree of anisotropy. The lower observed values depend also on specimen conditioning (i.e. defatting procedures). The Young's modulus measured in compression on cylindrical specimens from the bearing areas oriented perpendicular to the articular surface of the femoral head (Figure 6.4) suggests differences between the weight-bearing and partial weight-bearing head site [DEc].

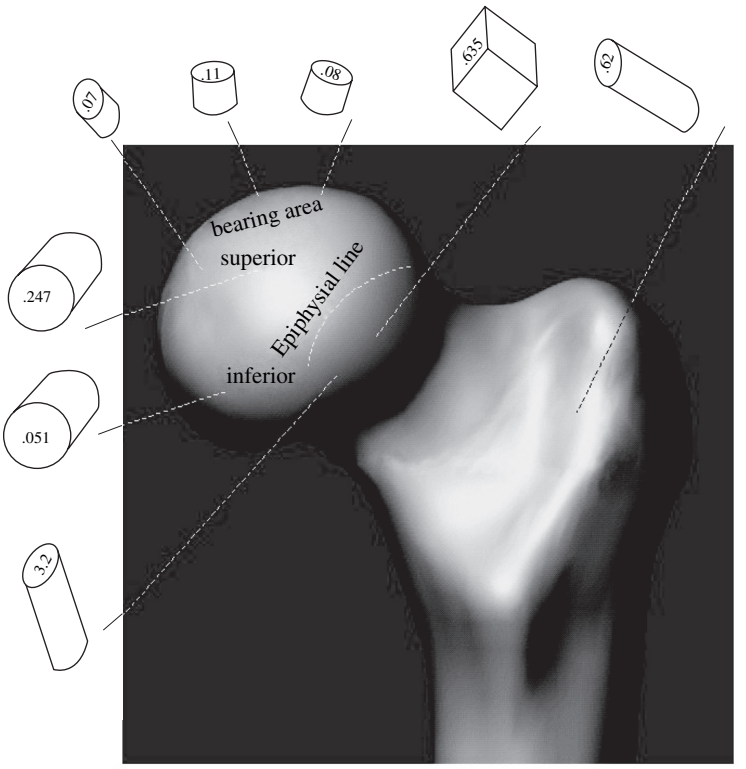

Figure 6.6. 3-D imaging of a femur showing Young's modulus anisotropy and site dependence of trabecular bone. Values are expressed in GPa [VAc, CIa].

Of course, the differences in the measured elastic property are also related to the mechanical preconditioning. Higher values of the elastic modulus are measured in the linear region of the stress–strain curves [CIa, HOb], or after a dynamic creep conditioning at low load levels [AUa, MAa].

Using a 5-mm gauge length extensometer and specimens oriented in the main direction of the trabecular network from the femoral neck, frozen and low strain conditioned bone shows moduli of 3.23 GPa and 2.7 GPa in compression and tension, respectively. The greater trochanter has an elastic modulus of about 0.6 GPa in both compression and tension-loading mode [MOa]. In contrast, nanoindentation measurements of trabecular bone from the femoral neck give a value of 11.4 GPa for the tissue modulus [ZYa]. Indeed, micro-FEM investigations use a uniform Young's modulus value for the trabecular bone material of between 10 and 18 GPa [BAd, ULa], in order to match the macroscopic apparent tissue modulus derived

Site	Dir.	Meth.	Y. Stress (MPa)	Y. Strain (mm/mm)	U. Stress (MPa)	U. Strain (mm/mm)	Ref.
Neck	IS	C	17.45	0.85 %			Morgan Keaveny 01
Neck	IS	T	10.93	0.61 %			
Prox. Femur	IS	C			2.9	3.2 %	Augat et al. 98
Dist. Femur	IS	C			2.2	2.9 %	
Sup. Head	AP	C			2.35		Brown et al. 02
Inf. Head	AP	C			0.56		
Prox. Femur	IS	C			2.5		Majumdar et al. 98

Table 6.3. Mechanical properties derived from destructive tests. (C = compression; T = tension; AP = anterior–posterior; IS = inferior–superior.)

from experimental investigations. Table 6.3 summarizes the mechanical properties derived from destructive tests.

6.2.4 Trabecular Bone from the Mandible

This site is of enormous importance for the outcome of prosthetic reconstructions with dental implants. The principal orientations of the trabecular network are affected by the teeth: mandible joint and the adaptation and remodeling consequent to chewing.

Compression tests on cubic specimens, whose sides are smaller than 5 mm, harvested from human edentulous mandible [OMa] show that a remarkable anisotropy exists in the premolar-incisal regions of the mandible arch (Figure 6.7). Compression tests on cylindrical specimens with similar dimensions from frozen mandibles aged between 56 and 90 years suggests an increase of the elastic modulus in the inferior-superior direction and a further decrease in the molar region [MIb]. It is also observed that the elastic modulus derived from unconfined or unconstrained compression tests lead to values that are about 40% lower than those detectable through constrained tests. An anisotropy in the elastic modulus of trabecular bone from the mandible condyle is apparent from compression tests on cylindrical specimens. Modulus values of 0.431 GPa and 0.127 GPa are exhibited in the superior–inferior and medio–lateral directions, respectively [GIa].

6.2.5 Anisotropy in the Elastic Modulus of Trabecular Bone

Based on the previous database of elastic modulus values it is possible to investigate the anisotropy of trabecular bone tissue according to the organ and the site. To do this the E_3/E_2 and E_3/E_1 ratios are considered. A first advantage of considering the anisotropy ratios is that a higher consistency

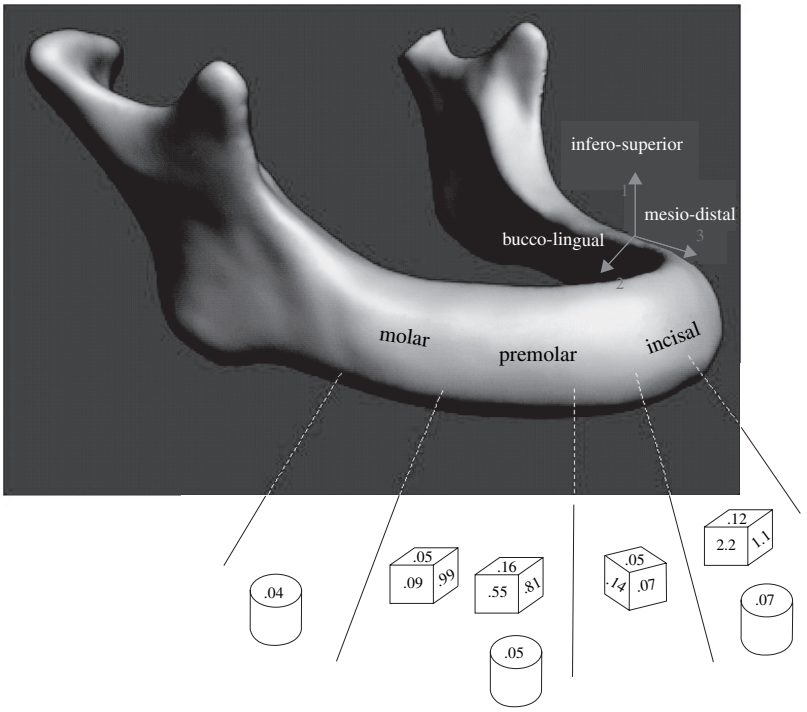

Figure 6.7. 3-D imaging of a mandible showing Young's modulus anisotropy and site dependence of trabecular bone. Values are expressed in GPa [OMa].

of the results is expected. These ratios are, of course, less sensitive to the specimen geometry and the mechanical testing setup.

It is interesting to observe from Table 6.4 that a higher anisotropy exists in the proximal tibia than in the proximal femur. Also, the vertebral trabecular bone displays a higher anisotropy than the proximal femur. However, compression tests on trabecular bone from the distal femur indicate an anisotropy ratio between the cephalo–caudal and medio–lateral direction of 3.5 [AUa]. Tibia, femur, and vertebra show that the highest elastic modulus is obtained in the cephalo–caudal or superior–inferior direction, and the anisotropy ratios with respect to the orthogonal directions (directions 1 and 2 of Figures 6.2, 6.3 and 6.4) are similar. This suggests that these sites can be modeled as transversely isotropic materials as a first approximation. The mandible, however, displays a completely different anisotropy. In each site the elastic modulus is higher in the mesio–distal direction, that is, the axis of the mandibular arch. Moreover, a higher anisotropy is observed compared to the trabecular bone from other organs.

Organ	Method	Site	c—Anisotropy		
			E_3/E_2	E_3/E_1	
Tibia	US	Subchondral bone plate	2.7–4.2	3.0–4.2	Rho et al. 96
		Middle bone plate	3.9–4.2	4.3–4.5	
		Deep bone plate	3.0–3.1	3.2–3.3	
Vertebra	MC	Central body L4	3.8	3.2	Nicholson et al. 98
		Central body L1	2.5	2.2	Augat et al 98
		Vertebral body	1.8	1.8	Hengsberger et al. 02
	US	Central body	1.3	1.3	Nicholson et al. 98
		Vertebral body	1.0	1.0	Hengsberger et al. 02
	NI	Axial trabeculae	0.8	—	Roy et al. 99
Femur	MC	Proximal femur	2.3	2.5	Augat et al. 98
		Proximal femur	2.5	2.2	Majumdar et al. 98
		Femoral head*	2.2	4.0	Deligianni 91
Mandible*	MC	Incisal	2.0	18	O'Mahoney et al. 00
		Canine	2.0	2.8	
		First premolar	1.5	5.1	
		Second premolar	11.0	19.8	
		condyle	3.4	—	Giesen et al. 01

Table 6.4. Anisotropy ratios of trabecular bone from different organs. (MC = mechanical compression; US = ultrasound; NI = nanoindentation. *a local reference system is used with direction 3 being the osteon orientation.)

6.2.6 Viscoelasticity of Trabecular Bone

Time-dependent properties of trabecular bone have been observed, as the strain rate in static compression tests on human trabecular bone is varied. The ability of fresh vertebral bone to bear compressive stress in the superior–inferior direction is enhanced at high levels of strain rate [GAa]. A power law relating elastic modulus to strain rate is commonly observed. Assuming a cubic dependence of the elastic modulus from the apparent density, an exponent of 0.06 for specimens tested in confined compression [CAb] and an exponent of 0.05 [LIb] for tibial bone have been reported. An exponent of 0.1 is derived for vertebral bone [OUa]. The dependence of the elastic modulus from the strain rate is also strongly related to bone marrow, especially at high strain rates. At a strain rate of 10 s^{-1}, both the elastic modulus and strength measurements of bone with marrow are about five times higher than those of bone without marrow. This suggests that marrow is a dominant factor controlling the mechanical behavior of bone. However, at strain rates lower than 1 s^{-1}, the effect of bone marrow is far less evident. Moreover, it has been pointed out that the effects of viscous flow of bone marrow on mechanical properties depend upon boundary conditions. Trabecular bone in vivo is confined by cortical bone, with the marrow therefore acting as an incompressible fluid, redistributing the stress to the trabecular network and thus increasing bone strength and modulus. In contrast to this, in vitro testing is generally carried out in unconfined conditions where, at low strain rates, marrow can flow through the pores and exit the specimen. In vitro testing at high strain rates provides a better representation of confined conditions [CAb]. In order to describe

the viscoelastic features of trabecular bone, stressed within physiological limits, a first approximation model is to consider trabeculae as elastic and the remaining material as a Maxwell body. This simplified model suggests that, during impact loading, the viscous marrow bears up to 30% of the applied load [KAa].

The effect of a fluid phase filling the bone porosity on the viscoelastic properties of human trabecular bone from the femoral head has also been detected through stress relaxation tests in compression [SCb, DEd]. By performing repeated stress relaxation tests at a fixed strain level, a higher stress decay is measured during the first test. However, no difference in the stress decay is observed through repetitive tests, if specimens are left to recover in Ringer's solution for 24 h. Moreover, a nonlinear viscoelastic behavior and a marked anisotropy for the relaxation constants are observed [DEd]. The viscoelastic properties of trabecular bone are more sensitive to storage conditions than is the elastic modulus. Defatting procedures lead to a 50% decrease in the viscoelastic energy dissipation [LIc]. Also, creep tests on trabecular bone from the femur suggest that time-dependent properties are a function of the site [ZIa]. Creep tests at low loading levels on trabecular bone from a vertebral body suggest a nonlinear viscoelastic behavior. Moreover, a full recovery of the strain is obtained only over a period 20 times longer than the duration of the creep test [YAa].

6.3 Cortical Bone

Cortical or compact bone constitutes the outer shell of bony organs such as the tibia, the femur, the vertebra, and the mandible. Osteons or the Haversian systems are the basic elements distinguished at a microscopic level. An osteon is generally an arrangement of concentric lamellae, each comprising mineralized collagen fibers oriented according to determined patterns, its shape approximating a cylinder. A more random organization of the mineralized collagen fibers distinguishes the woven bone (e.g. the bone in the callus). In long bones, the osteons are mainly oriented in the longitudinal direction and the peripheral osteons present their outer lamellae almost tangential to the external surface, forming, together with woven bone, a plywoodlike structure. This is a thick layer that represents, at a macroscopic level, the basic outer lamellar bone. This material is also the fundamental structural element of cementum, the material which coats the tooth's root and interfaces itself with periodontal ligaments in the alveolar bone. Orthogonal "plywood" structure is present in the outer lamellae of long bones [WEa]. The interface between osteons and bone matrix is the

cement line, which represents a region of reduced mineralization [BUb]. The cement line provides a ductile interface that promotes crack initiation but slows crack growth.

Imaging of cortical bone through a polarized light microscope suggests that the appearance of lamellae depends on the collagen fibers' orientation. In dark osteons, the lamellae are almost orthogonal to the plane of section—that is, parallel to the osteon axis—whereas in light osteons, the fibers are oriented almost parallel to the plane of section [EVa]. It has also been observed that transversely oriented collagen fibers prevail in regions of compact bone adapted to high compression stress, whereas longitudinal fibers are abundant in regions corresponding to high tensile stresses [BRa].

6.3.1 Elastic Properties of Cortical Bone at a Macroscale Level

It is not surprising that almost all of the research on mechanical properties of hard tissues developed during the last century focused on cortical bone. Compared to trabecular bone, this tissue is dense, so measurement errors related to porosity are reduced. Moreover, the fabrication of trabecular bone specimens generates peripheral artifacts caused by the fracture of trabeculae along the specimen's edges. Instead, the human body presents several sources from where cortical bone can be harvested in order to obtain specimens for standard mechanical characterization at the continuum level. Classical mechanical testing (compression, tension, bending, torsion, etc.) on cortical bone suggests the use of specimens that contain several Haversian systems. For this, a minimum cross-sectional area of 4 mm^2 is recommended [REa]. Through uniaxial tests on cortical bone from the middle one-third of the diaphysis of fresh femur, an average value of 17.1 GPa has been recorded. No difference has been observed between the tensile and compression-loading modes. The mechanical anisotropy of cortical bone has been investigated using several techniques. With piezoelectric transducers and sensors, a fast decrease of the Young's modulus from about 17 GPa to 14 GPa has been observed through a slight decrease of the specimen orientation with respect to the longitudinal axis of the femur [BOb]. An inconsistency is observed between the experimental data and the predictions of composite models based upon a simple linear superposition principle of collagen and apatite. Subsequently, using a hierarchical material-structure composite model, the variation of the Young's modulus with specimen orientation is explained [KAc]. Because compact bone is quite stiff, physiological loads usually produce small deformations, thus linear elasticity can be used to describe the mechanical behavior of compact bone.

The general linear elastic relationship between stress and strain ($\boldsymbol{\sigma} - \boldsymbol{\epsilon}$) is given by the tensorial form of Hooke's law

$$\boldsymbol{\sigma}_{ij} = \mathcal{C}_{ijkl}\boldsymbol{\epsilon}_{kl},$$

where $\mathcal{C}_{ijkl}$ is the elastic modulus tensor (the stiffness matrix) characterized by 81 elements. However, cortical bone can usually be assumed to behave as an orthotropic material, therefore only 9 independent constants can be distinguished. The compliance tensor for these model is given by:

$$S_{ij} = \begin{pmatrix} \frac{1}{E_1} & \frac{-\nu_{21}}{E_2} & \frac{-\nu_{31}}{E_3} & 0 & 0 & 0 \\ \frac{-\nu_{12}}{E_1} & \frac{1}{E_2} & \frac{-\nu_{32}}{E_3} & 0 & 0 & 0 \\ \frac{-\nu_{13}}{E_1} & \frac{-\nu_{23}}{E_2} & \frac{1}{E_3} & 0 & 0 & 0 \\ 0 & 0 & 0 & \frac{1}{G_{23}} & 0 & 0 \\ 0 & 0 & 0 & 0 & \frac{1}{G_{31}} & 0 \\ 0 & 0 & 0 & 0 & 0 & \frac{1}{G_{12}} \end{pmatrix},$$

where E_i, G_{ij}, and ν_{ij} are the elastic moduli, the shear moduli, and the Poisson ratios, respectively. The directions 1, 2, and 3 are the transverse, radial, and longitudinal directions, respectively. The elastic constants of the stiffness matrix are given by

$$C_{11} = \frac{1-\nu_{23}\nu_{32}}{E_2E_3\Delta}, \quad C_{22} = \frac{1-\nu_{13}\nu_{31}}{E_1E_3\Delta}, \quad C_{33} = \frac{1-\nu_{12}\nu_{21}}{E_1E_2\Delta},$$

$$C_{12} = \frac{\nu_{12}-\nu_{32}\nu_{13}}{E_1E_3\Delta}, \quad C_{13} = \frac{\nu 13-\nu_{12}\nu_{23}}{E_1E_2\Delta}, \quad C_{23} = \frac{\nu 23-\nu_{21}\nu_{13}}{E_1E_2\Delta},$$

$$C_{44} = G_{23}, \quad C_{55} = G_{31}, \quad C_{66} = G_{12},$$

$$\Delta = \frac{1-\nu_{12}\nu_{21}-\nu_{23}\nu_{32}-\nu_{31}\nu_{13}-2\nu_{21}\nu_{32}\nu_{13}}{E_1E_2E_3}.$$

Often, bone can be adequately described as a transversely isotropic material, because an axis of material symmetry can usually be recognized. Thus the number of independent constants reduces to five and the compliance tensor is characterized by the following relationships: $E_1 = E_2$, $\nu_{31} = \nu_{32}$, $\nu_{12} = \nu_{21}$, $G_{31} = G_{23}$, and $G_{12} = E_1/2(1+\nu_{12})$. Mechanical tests employing the strain gauge technique and continuous acoustic measurements have been the first methods to measure the mechanical anisotropy of human femoral cortical bone. Experimental mechanical testing aimed at determining five elastic constants are depicted in Table 6.5.

Ultrasonic data on cortical human bone from the tibia and mandible also support the hypothesis of an orthotropic anisotropy of cortical bone (Table 6.5). Nevertheless, the data presented in Table 6.5 are simplified,

Year	1975		1984	1987	1996				2003		
Organ	Fm		Fm	Fm	Tb				Mn		
Site					An	Lt	Ps	Md	Al	Ib	Sy
Meth.	M		U	M	U				U		
Mode	C	T		T							
E_1 [GPa]	18.2	17.7	20.0	22.5	20.9	20.6	21.1	21.2	25.2	23.0	21.1
E_2 [GPa]	11.7	12.8	13.4	13.4	11.5	11.9	12.3	12.9	12.7	16.0	16.8
G_{12} [GPa]	3.3	3.3	6.23	6.23	5.5	5.7	5.8	6.1	6.8	7.2	7.4
ν_{12}	0.63	0.53	0.35	0.32	0.40	0.40	0.40	0.38	0.41	0.34	0.41

Table 6.5. For the sake of simplicity only four of the measured elastic constants are reported [REb, ASe, DAa, RHd, SCc]. Direction 1 stands for the axis of material symmetry. (Fm=femur; Tb=Tibiae; Mn=mandible; A=anterior; L=lateral; P=posterior; M=medial; Al=alveolar; I=inferior border; S=symphysis. C and T denote compression and tension, respectively. M and U denote mechanical and ultrasound testing, respectively.)

consistent with the case of transverse isotropy. Table 6.5 shows the dependence of the elastic constants on the organ and site. It is interesting to note that, compared to investigations on trabecular bone, local elastic properties measured by applying AFM and SAM techniques to single osteons provide slightly higher values [TUa] than traditional mechanical measurements, namely direct mechanical testing and ultrasound, on cortical bone.

A detailed map depicting the spatial distribution of the Young's modulus during bending of cortical bone tissue from the femoral midshaft along the longitudinal direction is shown in Figure 6.8 [CUa]. Specimens with a thickness of 1 mm were obtained through serial cutting of the femoral shaft with a diamond saw. A span of 30 mm is used for a three-point bending test. Elastic values range from 14.0 to 22.8 GPa, with an average value of 18.6 GPa.

6.3.2 Yield and Failure Properties of Cortical Bone

Yield and failure properties of materials are determined through direct mechanical testing according to the traditional tensile, compression, bending, and torsion tests. Inasmuch as it is impossible to determine exactly the linear elastic limit of a material, a yield point is defined as the intersection of the stress–strain curve and a straight line whose slope is the Young's modulus of the material and which is positioned at 0.2% strain offset from the origin. Ultimate properties refer to the stress and strain of the maximum stress point, which in the case of cortical bone coincides with the point of rupture of the stress–strain curve.

Table 6.6 shows yielding and failure properties of human compact bone from the femur. It is apparent that higher values of ultimate strength in tension and compression are observed along the longitudinal direction.

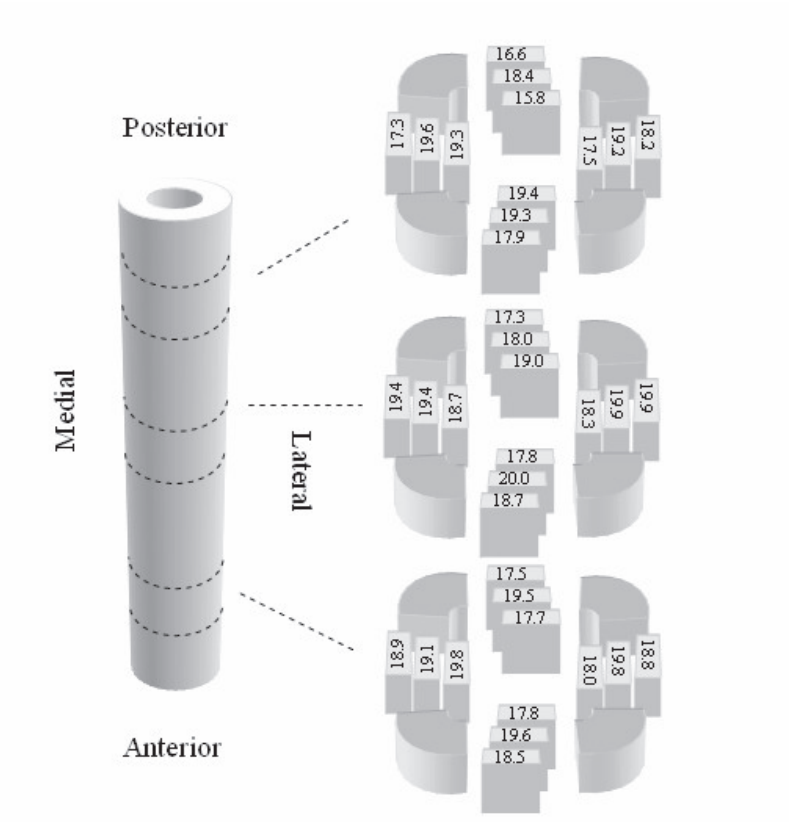

Figure 6.8. Map of the Young's modulus in bending of cortical bone tissue from the femoral midshaft along the longitudinal direction [CUa].

Reference	Reilly and Burstain 75					Bayractar04	Curre04	Jepsen97
Test	Tension		Compression		Shear	Tension	Bending	Torsion
Direction	Long.	Trans.	Long.	Trans.	Trans.	Long.	Long.	
Y. Strain [mm/mm]						0.73 %	1.41%	1.3 %
Y. Stress [MPa]						107.9		55.8
U. Strain [mm/mm]	3.8 %	0.7 %	1.9 %	0.5 %				5.2 %
U. Stress [MPa]	133	53	205	131	67		208	74.1

Table 6.6. Yielding and failure properties of human compact bone from femur.

Test	Property	Children	Young adult	Adult	Elderly	Ref.
T	Modulus [GPa]		15.69		14.78	Courtney et al 96
T	Yield Strain [mm/mm]		0.378 %		0.356 %	
T	Yield Stress [MPa]		55.3		49.3	
T	Failure Stress [MPa]		81.6		78.7	
T	Failure Stress [MPa]	114	122	102	86	Natali Hart 02
C	Failure Stress [MPa]		167	158		
B	Failure Stress [MPa]	151	173	158	139	
S	Failure Stress [MPa]		57	52	49	

Table 6.7. Effects of age on the mechanical properties of cortical bone from the human femur. (T=tension; C=compression; B=bending; S=Shear (torsion).)

Direction	Children	Adult	Ref.
0°	12.8	17.5	Hara et al. 98
30°	9.9	14.3	
60°	5.4	11.7	

Table 6.8. Effects of age on the elastic modulus of cortical bone from the mandible in bending.

The effects of age on mechanical properties of human cortical bone have also been investigated. Generally, these properties increase from the child (5–20 years) to the young adult (20–40 years), decrease slightly in the adult (40–60 years) and then decrease more markedly in the elderly person (60–80 years). Table 6.7 illustrates the effects of age on the mechanical properties of cortical bone from the human femur in tension compression, bending, and torsion, and Table 6.8 illustrates the same effects concerning the elastic modulus in bending of the mandible at various angles.

6.3.3 Viscoelasticity of Cortical Bone

The mechanical properties of human cortical bone depend on strain rate in the sense that a higher strain rate produces a higher elastic modulus, thus suggesting that cortical bone behaves as a viscoelastic material [MCa]. As with trabecular bone, the viscoelastic properties of cortical bone are strongly dependent upon the water phase. Dynamic mechanical analyses (DMA) at 1 Hz and 37°C on 3P-bending specimens of human cortical bone from the tibia (Table 6.9) suggest that water mainly affects the damping factor, and therefore the loss modulus, rather than the storage modulus [YAb]. The effect of interstitial fluid flow on hydraulic strengthening of bone has been analyzed through nonlinear models. It is suggested that a window of strain rates exists between 10^{-3} s^{-1} and 10^{+3} s^{-1}. Within this window, the loss tangent is higher at low and high strain rates. Outside the boundaries of this strain rate range, there are no further strengthening effects on fluid flow resulting from recourse to higher or lower strain rates [LIa].

Reference		Yamashita 00	Bargren 74		FanRho 02		
	Conditions	Bending	Compression		AFM		
Freq./Load		1 Hz	5.2 Hz	7.5 Hz	10 μ N/s	$10^2\mu$ N/s	$10^3\mu$ N/s
					18.6	26.5	32.2
Storage	0° wet	9.4					
Modulus	0° dry	9.4					
[GPa]	0°		15.8	16.3			
	30°		10.8	11.4			
	45°		12.5	12.4			
Damping	0° wet	0.041					
factor (tan δ)	0° dry	0.029					

Table 6.9. Viscoelastic properties of cortical bone. Data from Bargren et al. 1974 are converted in standard units.

Anisotropy in viscoelastic properties is, of course, often observed. The data in Table 6.9 clearly illustrate that both the storage and loss moduli of cortical bone from the diaphysis of a human femur (from a woman, age 26 years) are greatest in the longitudinal direction [BAc]. Furthermore, both these moduli increase with increasing frequency. The increase in the elastic modulus has also been observed through AFM, performing viscoelastic measurements by changing the stress rate of the loading–unloading cycles of the tip indenter [FAa].

6.3.4 Fracture Mechanics

Bone undergoes microcracking as a result of repetitive daily stress while, simultaneously, the remodeling process occurs, establishing an equilibrium in the microcrack density within the living tissue [LAa]. The microstructure of bone anyway provides sites of discontinuity—including lacunae, canaliculi, blood vessels, and muscle insertions—all of which act as stress raisers [CUb]. The dimensions of intrinsic crack initiation sites are, for example, of the same order as those of the vascular spaces [BOa]. An in vitro comparison of the fracture mechanisms of human cortical bone suggests that the microcracks which form around a cracktip redistribute the stresses, increasing the toughness of the material [SIb, VAd].

Fracture toughness capability of Haversian bone is related to the osteonal structure. Similar examples among engineering materials are tough discontinuous fiber-reinforced laminates [NIc, NOb]. A ductile osteon–matrix interface—the cement line—promotes crack initiation [EVa], but slows crack propagation in compact bone [BUb] by blunting the crack tip and trapping it within the lamellar structure. A bridging effect of osteon is observed for cracks propagating in the osteon orientation [DEb].

Debonding of an osteon produces changes in the region of the Haversian canal wall adjacent to the crack, such as interruption of streaming potentials and nutrients. This debonding initiates remodeling and production of a new

Site	Geometry	Direction	Speed	$K_c[MNm^{-3/2}]$	References
Tibia	SEN	longitudinal	Fast	2.2–4.6	Bonfield Datta 76
Tibia	CT	longitudinal	Slow	2.1–4.7	Behiry Bonfield 84
Tibia	CT	longitudinal	Slow	4.48	Norman et al 91
Tibia	CT	longitudinal	Slow	4.05	Norman et al. 95
Tibia	CT	longitudinal	Slow	2.08	Norman et al. 96
Tibia	CS (mode II)	longitudinal	Slow	8.32	Norman et al. 96
Femur	CT	longitudinal	Slow	1.6–2.5	Vashishth et al. 97
Femur	CT	longitudinal	Slow	1.71	Akkus et al. 00
Femur	CT	transverse	Slow	3.47	Akkus et al. 00

Table 6.10. Stress intensity factor of human cortical bone.

secondary osteon, initially less calcified than the surrounding bone [SIb], which may act as a fiber reinforcement [BUb] preventing the accumulation of microdamage due to repetitive loading [MAd].

Micromechanical models of osteonal cortical bone suggest that the ratio of the modulus of the osteon to that of the interstitial bone controls crack propagation. Newly formed, low-stiffness osteons may toughen cortical bone by promoting crack propagation toward tougher osteons whereas stiff osteons repel the microcrack from more brittle osteons [GUa]. With aging, microdamage occurs more rapidly than the intrinsic repair process [SCa]. The effects of this accumulation of microcracks, which is higher in females than males [NOd], are reduced mechanical properties and increased fragility [COa, MAe]. Thus bone fracture has an increased occurrence within older persons because the microstructural organization of bone controls the relationship between loading conditions and fracture patterns [EVa, CLa]. Hence fracture toughness plays a decisive role in bone functionality by determining the level to which the material can be stressed in the presence of cracks, or, equivalently, the magnitude of cracking that can be tolerated at a given stress level.

Almost all of the literature data on fracture mechanics of cortical bone are based on the CT specimen and mode I condition. Table 6.10 shows the stress intensity factor of human cortical bone. In particular, it is suggested that fracture toughness of cortical bone in the osteonal direction is higher in shear than in tension [NOc]. Furthermore, fracture toughness in the transverse direction is higher than in the longitudinal direction [AKa].

6.3.5 Fatigue of Cortical Bone

Several fatigue investigations have been carried out on cortical bone through in vitro testing. It must be noted that the fatigue behavior of living bone is not known, and that the in vitro testing of cortical bone does not consider the remodeling process. Therefore, care has to be taken when transferring in vitro results to in vivo behavior of bone and failure predictions.

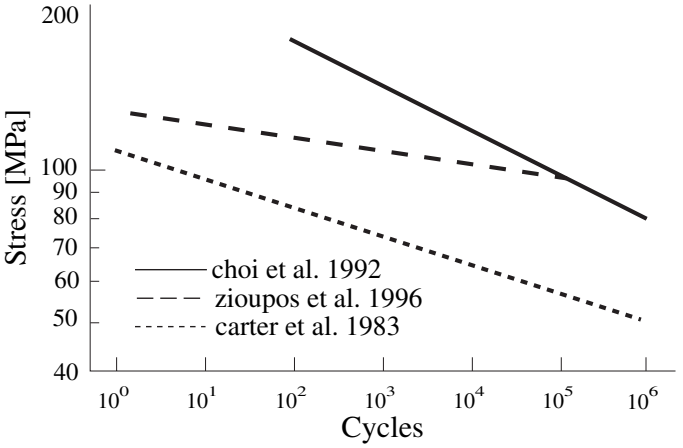

Figure 6.9. Fatigue behavior of cortical bone.

The osteoclast and osteoblast activity controls the extracellular matrix absorption or production, respectively. Therefore, it has been suggested that the Woehler S–N diagrams in Figure 6.9 have to be interpreted as a lower bound limit if the osteoblast activity is the dominant process, and an upper bound limit if the resorption process prevails [KEb]. In general, dynamic sinusoidal stress is applied at 2 Hz. Figure 6.9 reports the S–N diagrams of human cortical bone. Human cortical bone (average 69-year-old) cyclically stressed in tension at 37°C has provided lower fatigue strength values than bone (average 27-year-old) at 25°C [CAc, ZIb]. A different fatigue behavior is observed using the four-point bending method for bone tested at 25°C [CHc].

6.4 Dental Tissues

The dental tissues consist of enamel, dentine, cementum, and the pulp. The arrangement of the hard materials is depicted in Figure 6.10, where the junctions, CEJ (cementum–enamel junction) and DEJ (dentine–enamel junction), can be clearly distinguished.

Dentine forms the bulk of the tooth. Like compact bone, it comprises an inorganic mineral component, hydroxyapatite, and an organic matrix, which is mainly collagen. Again, as with bone, type I fibrillar collagen is the main constituent of the extracellular matrix of dentine. However, it has been established by chromatography that dentine collagen exhibits a cross-link distribution different from that of bone collagen [KUa]. Dentinal

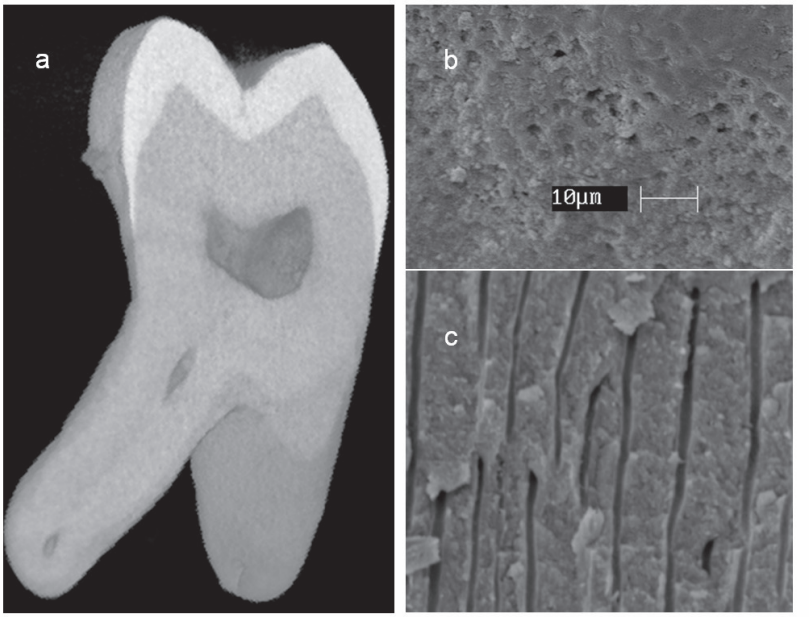

Figure 6.10. (a) 3-D reconstruction of a micro X-ray CT of a human third molar; (b) SEM image of a horizontal section from the dentine crown; (c) SEM image of a longitudinal section from the dentine crown (courtesy of Dr. D. Prisco, School of Dentistry, University of Naples Federico II, Naples, Italy.)

tubules across dentine [VEa] and the intertubular and peritubular dentine (ITD and PTD, respectively) may be distinctly identified. Dentinal tubules permeate through dentine, their pattern following an S-shaped curvature. Lateral branches of the tubules, with a smaller diameter, complete the network [CAa]. There is a different distribution of dentinal tubules and diameter in the pulp–DEJ direction [GAb]. The tubules are wider and more numerous near the pulp.

Enamel covers the crown of the tooth, and its structure consists of tightly packed hydroxyapatite crystals. These are organized in highly oriented patterns, forming enamel rods. These rods, which extend from the DEJ to the surface of the enamel, are arranged in circumferential rows around the main axis of the tooth.

Dentine and enamel are 65% and 95–98% mineralized, respectively. It should be noted that mature enamel is not a living tissue. Compared to dentine, enamel is harder but also more brittle. Moreover, thermal properties suggest that enamel has a higher coefficient of thermal conductivity

than dentine. The overall natural organization of dentine and enamel is optimized in order to perform thermomechanical functions [CRb].

The pulp, which is richly innervated, is the soft tissue of the tooth. It occupies the central portion of the tooth represented by the coronal pulp chamber and the radicular root canal. Vessels enter into the pulp through the apical foramina. The principal cells of the pulp are the odontoblasts, whose processes extend into dentine.

Cementum covers the root of a tooth; it is a bonelike structure. This tissue is deposited as a thin layer from the CEJ to the apex of the tooth; this layer thickness is higher at the apex. Cementoblasts and cementocytes are the cells of cementum, however, unlike bone, cementum is avascular and incapable of remodeling. Cementum anchors the tooth to the surrounding alveolar bone through the periodontal ligament.

The periodontal ligament system comprises soft, fibrous connective tissue, which extends from the cement of the root to the alveolar bone, following an obliquely cervical direction. The periodontal ligament characterizes the joint between the tooth and the alveolar bone. Periodontal ligaments also act as a natural shock-absorbing system.

6.4.1 Elastic Properties

Dentine, like compact bone, is a heterogeneous multiphase material that exhibits a hierarchical composite structure. Therefore, like bone, mechanical properties depend on the scale level at which properties are measured. Also, experimental measurements are sensitive to the specimen source and testing conditions.

The Young's modulus of dental hard tissues, similarly to that of bone, is confined between upper and lower bounds related to the stiffness of hydroxyapatite and collagen, respectively. Given the geometrical constraints pertaining to dental hard tissues, it is very difficult to harvest specimens of appropriate dimensions in order to carry out classical mechanical testing. Therefore, the testing of dentine with dynamometers is generally performed using micromechanical methods. Specimen volumes are typically of the order of a few cubic millimeters, with cross-section areas often less than 1 mm^2 for tensile tests [SAa]. Data from measurements of the Young's modulus of dentine are presented in Table 6.11.

Reference	CraigPey 58	Tylesley 59	BowenRod 62	RensonBra 75
Testing Mode	Compression	4-Point Bending	Tension	Cantilever
Young's modulus [GPa]	18.3	12.3	19.3	11.1–19.3

Table 6.11. Young's modulus of dentine.

Temperature	0°C	23°C	37°C	50°C	80°C
Young's Modulus [GPa]	15.20	13.94	13.26	12.06	9.35

Table 6.12. Dependence of Young's modulus of dentine on temperature [WAb].

The mechanical properties of demineralized dentine are of great importance. Most of the bonding systems used in restorative dentistry are carried out through the etching of dentine, which has the effect of removing the mineral phase of the tissue. The Young's moduli in tension of mineralized and demineralized human dentine are 13.7 GPa and 0.25 GPa, respectively [SAb]. The temperature-dependence of the elastic properties of dentine are also notable. In contrast to bone tissue, which experiences a rather constant temperature, dental tissues are thermally stressed over a wider temperature range. Table 6.12 shows the dependence on temperature of Young's modulus in compression [WAb].

In each tooth, there is a variability in the mechanical properties of dentine. Anisotropy and inhomogeneity are induced by the tubules network, varying distributions of both intrafibrillar, and extrafibrillar minerals, and water content, inter alia. Variations are also observed among different teeth. Therefore, mechanical properties of dentine are site-dependent, and the elastic moduli measured through classic mechanical tests have to be interpreted as average values. The properties of caries-affected dentine are very important. This degenerated tissue is less stiff and contains more water than normal dentine [ITa].

Indentation tests are an alternative to classical micromechanical testing, permitting a detailed mapping of dentine and enamel elastic properties. The average values of Vickers' hardness of dentine and enamel are 57–60 kg/mm^2 and 294–408 kg/mm^2, respectively [WIb, FOb]. The averaged Young's moduli (derived from Vickers' hardness, assuming a Poisson ratio of 0.25) of enamel in the axial and transverse directions are 94 GPa and 80 GPa, and the modulus that has been derived for dentine is 20 GPa [XUa]. The Young's modulus of dentine derived from microindentation through a Knoop indenter decreases toward the DEJ. Using a proportional constant of 0.45 between Young's modulus and Knoop hardness, the elastic modulus decreases from 11.2 GPa at a distance of 2.5 mm to 8.7 GPa close to the DEJ [MEb]. Also, microindentation measurements suggest that the elastic modulus of dentine decreases toward the DEJ. Furthermore, gradients in the Young's modulus have been detected also in the facial–lingual direction [KIf].

It is important to notice that hardness measurements through indentation testing are strongly dependent on the size of the indenter. The

impression size in dentine using traditional indenters (e.g. Vickers, Knoop, etc.) is of the same order as heterogeneities such as enamel rods or dentinal tubules, preventing accurate assessment of material properties. Using AFM, the elastic moduli derived from nanoindentation are 19.3 GPa and 90.6 GPa for dentine [VAb] and enamel [WIc], respectively. The hardness of hydrated PTD and ITD are 2.3 GPa, and 0.5 GPa, respectively [KIa]. A drawback in early AFM measurements was the inability to keep specimens wet during testing. Using modified AFM, it has been possible to apply loads in the range of 1 μN to 100 N through the tip of the indenter on fully hydrated specimens [BAa]. The Young's modulus in the axial direction increases monotonically from 15.3 GPa near the DEJ to 16.3 GPa at a distance of about 1 mm from the pulp. Also, a rapid decrease of the ITD Young's modulus is observed as dentine absorbs water from the dry state to the rehydrate state [KIc].

It is suggested that the dependence of mechanical properties of dentine from the site is related to mineral content and crystal thickness. Dentine exhibits minimum values of hardness and elastic modulus close to the DEJ. Towards the DEJ, the mineral content decreases and the crystal thickness increases [TEa].

Several AFM studies are reported regarding the gradient properties across the dentine–DEJ–enamel regions, the results showing general agreement. The Young's modulus gradually increases through the DEJ region (with a thickness of about 10 μm), increasing from about 20 GPa in the dentine region to about 80 GPa in the enamel region [MAb, FOa, MAc, BAb]. The anisotropy in the mechanical properties of dentine derives from the ultrastructural organization of collagen fibrils and mineral crystals. The contribution of collagen to the elastic modulus of enamel is negligible, and even viscoelastic properties do not change across the enamel region. Dentine strength, toughness, and bonding performances, on the other hand, are dependent on the collagenic network properties. Surprisingly, resonant ultrasound spectroscopy suggests that dentine is stiffer in the direction perpendicular to the tubules. The derived values for the Young's modulus in the axial and transverse directions are 23.2 GPa and 25.0 GPa, respectively, which would be consistent with cuffs of PTD and collagen fibrils that lie in planes transverse to each tubule axis [KId].

The size of human enamel specimens available for testing does not allow the measurements of elastic properties according to standard mechanical tests. Therefore, almost all of the literature concerning fracture properties of enamel refers to indentation techniques. AFM measurements through nanoindentation provide an excellent tool to distinguish the site-dependence properties and the anisotropy of human enamel. The Young's modulus, derived from nanohardness measurements assuming a

Poisson ratio of 0.28, is higher in the direction parallel to enamel rods (E = 87.5 GPa). In the direction parallel to enamel rods the derived Young's modulus is 72.7 GPa, therefore an anisotropy of about 30% is observed. Moreover, the elastic modulus is lower in both the tail and interrod enamel [HAb].

6.4.2 Ultimate Static Properties of Dentine

Concerning the harvesting of tissues for significant mechanical testing, third molars are the preferred specimen source, because dentine here is abundant in the crown region. Dentine specimens from the root of incisors and canines are also a popular choice. Hollow cylindrical specimens from the root site are likely to be axisymmetric, the tubules being almost perpendicular to the root axis. However, ultimate properties depend upon the organ, site, and orientation of tubules with respect to loading direction. The anisotropy and the site dependence of mechanical strength are shown in Table 6.13. It is interesting to observe that the tensile strength anisotropy, similarly to the elastic modulus, is such that strength is higher for specimens with tubules oriented perpendicular to the applied load; this is found for both root or crown dentine [LEb, MIa]. An increase of strength is measured toward the DEJ [STa, KOa]. Dentine close to the DEJ is less stiff but has a higher strength both in tension and in shear.

The anisotropy in tensile strength is also observed for demineralized dentine. Mid-coronal demineralized specimens contribute approximatively 30% to the strength of dentine with tubules oriented in the perpendicular direction [SAa]. The same result is found for root dentine [MIa]. Moreover, demineralized wet dentine shows a well-defined toe region and an ultimate strain that is one folder higher than mineralized dentine [SAb]. The yield strength in three-point bending of dentine from human molars is 75 MPa

Organ	Region	Mode	Tubule Orientation	Strength [MPa]	Reference
Third molar	Mid-Coronal	T	Perpendicular	105.5	Sano et al. 94
Incisor canine	Root	T	Parallel	41.1	Letchirakarn et al. 01
		T	Perpendicular	59.6	
Third molar	Middle cervical	T	Perpendicular	83.6	Staninec et al. 02
	Middle occlusal	T	Perpendicular	61.7	
Third molar	Outer coronal	S	Perpendicular	76.7	Konishi et al. 02
	Pulpal coronal	S	Perpendicular	52.7	
Molar	Coronal and root	B	Perpendicular	160	Imbeni et al. 02
Third molar	Coronal	T	Parallel	73.1	Miguez et al. 04
		T	Perpendicular	140.4	
	Root	T	Parallel	63.2	
		T	Perpendicular	95.9	

Table 6.13. Mechanical strength of dentine. (T = tension, S = shear, B = bending.)

Temperature	0°C	23°C	37°C	50°C	80°C
Compressive strength [MPa]	297	271	260	247	208

Table 6.14. Dependence of the compressive strength of dentine on temperature [WAb].

[IMa]. Table 6.14 shows the dependence on temperature of the compressive strength of dentine [WAb].

6.4.3 Viscoelastic Properties

The mechanical properties of dental tissues are time-dependent. For the case of the compressive elastic modulus, for instance, a power law is observed for hollow cylindrical specimens obtained from the root of incisors. The exponent (0.017) is towards the lower end of the range of values reported for bone. Moreover, the independence of the creep compliance from the applied stress suggests a linear viscoelastic behavior. The reduction in the relaxation modulus in water at 25°C after 1 hour is 6–17%, whereas at 37°C after six hours the reduction is 10–30% [DUa, JAa].

It must be borne in mind that viscoelastic testing, through creep or stress relaxation, generally implies long duration experiments. It is, therefore, important to consider the extent to which tissue degradation might occur over such periods. A 30% of reduction in the Young's modulus of dentine is reported for water storage, this reduction being ascribed to calcium phosphate dissolution. In order to collect reliable measurements over the course of long duration tests, the use of Hanks' Balanced Salt Solution (HBSS) is recommended [HAa, KId].

Viscoelastic measurements of demineralized dentine have been performed using both AFM and micromechanical axial tests [BAa, PAa]. The Young's modulus derived from AFM measurements of demineralized, dehydrated, and rehydrated dentine from the crowns of third molars are 149 kPa, 2.1 GPa, and 381 kPa, respectively. Viscoelastic behavior of fully demineralized dentine is observed, and it is suggested that collagen contribution to dentine modulus is negligible [BAa]. The low value reported for the modulus of demineralized dentine compared to other investigations [SAb] is ascribed to the testing method.

Viscoelastic behavior is also observed on demineralized dentine specimens from mid-coronal dentine, using tension and compression stress–relaxation and creep tests in a wet environment. In particular, stress relaxation and creep tests in tension suggest a linear viscoelastic behavior for demineralized dentine, whereas a different behavior is observed in compression because creep results are dependent on the applied stress [PAa]. Using nano-DMA via AFM, with the indenter modulated at 200 Hz, a complete

mapping of the storage and loss moduli of dentine and enamel have been obtained. Average storage moduli of 21 GPa and 63 GPa are measured for ITD and enamel, respectively. PTD displays a storage modulus higher than ITD. Moreover, the loss modulus of ITD is higher than those measured for PTD and enamel. This suggests a higher dissipation capability of ITD, which is consistent with the high concentration of collagen fibrils in the dentine matrix [BAb].

6.4.4 Fracture Properties

The fracture toughness of dentine is midway in the range observed for cortical bone (0.23–6.56 $\mathrm{MN/m^{-1.5}}$), and is at least one order of magnitude greater than dentine restorative materials [TAa]. Using the three-point bending technique on dentine specimens with a chevron notch in the middle section, the anisotropy in the toughness of dentine and enamel can be examined. For dentine, the work of fracture over a plane oriented parallel to the tubules is higher than that perpendicular to the tubules. On the other hand, for enamel, the work of fracture over a plane oriented parallel to enamel rods is lower than that measured perpendicular to the rods [RAa].

Using the CT geometry loaded as mode I of coronal dentine specimens, with tubules oriented parallel to the surface of fracture, it is suggested that fracture toughness is invariant with temperature ($\mathrm{K}_{Ic,37^{\circ}\mathrm{C}} = 3.1\ \mathrm{MNm^{-1.5}}$), whereas the strain energy release rate increases with temperature. Two toughening effects are suggested for the moderate level of fracture toughness shown by dentine for a crack propagating parallel to tubules. The first of these is the blunting of the tip of a propagating crack by each tubule that is crossed [ELa]. The second is the strengthening effect due to mineralized collagen fibrils, which form a planar, feltlike structure perpendicular to the tubules [NAb].

The dependence of fracture toughness upon the orientation of tubules has been observed also on dentine from human molars. Test specimens are shaped as notchless triangular prisms of dentine, inserted in a metal short rod CNT holder. Three tubule orientations have been tested: plane of crack propagation perpendicular, parallel, and parallel-transverse to the plane of dentinal tubules. Results indicate that the fracture toughness is 1.13 $\mathrm{MNm^{-1.5}}$, 2.02 $\mathrm{MNm^{-1.5}}$, and 1.97 $\mathrm{MNm^{-1.5}}$, respectively [IWa]. The anisotropy in elastic, ultimate, and fracture properties of dentine would certainly indicate that dentine is stiffer, stronger, and tougher for specimens with tubules oriented perpendicular to the applied load. By using the three-point bending method on dentine specimens from the coronal and root regions of human molars, with tubules oriented perpendicularly to the fractured surface, the measured fracture toughness is 2.72 $\mathrm{MNm^{-1.5}}$. However, it has been argued that these values of fracture toughness have to

be interpreted as an apparent value which overestimates by about 50% the real fracture toughness of dentine. In fact, by using the same test method on fatigue precracked samples, the real fracture toughness is found to be 1.79 $MNm^{-1.5}$ [IMa].

The size of human enamel specimen available for testing prevents the measurements of fracture toughness according to standard fracture tests. Therefore, almost all of the literature concerning fracture properties of enamel refers to indentation-fracture techniques. By using the microindentation technique, through a Vickers' indenter, the fracture toughness of human enamel differs for molar, incisor, and canine teeth, the lowest values being measured for molar enamel. For each tooth, fracture toughness of enamel increases in the incisal-cervical direction. The range of values observed is 0.7–1.27 $MNm^{-1.5}$ [HAd]. Similar values for the fracture toughness of human enamel, spanning from 0.61 $MNm^{-1.5}$ to 0.84 $MNm^{-1.5}$, have been measured using the indentation microfracture method, and higher values are detected in the direction of enamel rods [OKa].

6.4.5 Fatigue Properties

Several investigations have been carried out on dentine using in vitro testing. Compared to cortical bone, dentine is biologically less active. Consequently, the fatigue behavior of dentine, in vitro, should reflect more the effects of cyclic loading in vivo during mastication.

The fatigue behavior of dentine obtained from the crown and the root of human molars, with the tubules oriented perpendicularly to the applied stress and to the plane of the crack, has been investigated using cantilever geometry. Fatigue testing has been carried out in an HBSS environment. At room temperature, the endurance strength at 106–107 cycles, for a minimum to maximum stress ratio of 0.1, is 25 MPa and 45 MPa, for cyclic frequencies of 2 Hz and 20 Hz, respectively. Therefore, the fatigue behavior of dentine is time-dependent [NAb]. Under the same testing conditions, the endurance strength of dentine at body temperature cycling at a frequency of 10 Hz, reduces with increasing stress ratio. For a stress ratio of -1, the endurance strength is about 30–50% of the single-cycle tensile test, implying that dentine displays a metallike fatigue behavior [NAc].

6.5 References

[AKa] Akkus, O., Jepsen, K.J., and Rimnac, C.M., Microstructural aspects of the fracture process in human cortical bone, *J. Mat. Sci.*, **35** (2000), 6065–6074.

[APa] Apicella, A., Liguori, A., Masi, E., and Nicolais, L., Thick laminate composite modeling in total hip replacement, in **Experimental Techniques and Design in Composite Materials** Sheffield Academis Press, (1994), pp. 323–338.

[ASa] Ascenzi, A., Baschieri, P., and Bonucci, E., The bending properties of single osteons. *J. Biomech.*, **23** (1990), 763–771.

[ASb] Ascenzi, A. and Bonucci, E., The compressive properties of single osteons. *Anatom. Rec.*, **161** (1968), 377–391.

[ASc] Ascenzi, A. and Bonucci, E., The tensile properties of single osteons. *Anatom. Rec.*, **158** (1967), 375–386.

[ASd] Ascenzi, A., Benvenuti, A., Bigi, A., Foresti, E., Koch, M.H., Mango, F., Ripamonti, A., and Roveri, N., X-ray diffraction on Cyclically loaded osteons. *Calcif. Tissue Int.*, **62** (1998), 266–273.

[ASe] Ashman, R.B., Cowin, S.C., Van Buskirk, W.C., and Rice, J.C., A continuous wave technique for the measurement of the elastic properties of cortical bone. *J. Biomech.*, **17** (1984), 349–61.

[AUa] Augat, P., Link, T., Lang, T.F., Lin, J.C., Majumdar, S., and Genant, H.K., Anisotropy of the elastic modulus of trabecular bone specimens from different anatomical locations. *Med. Eng. Phys.*, **2** (1998), 124–31.

[BAa] Balooch, M., Wu-Magidi, I.C., Balazs, A., Lundkvist, A.S., Marshall, S.J., Marshall, G.W., Siekhaus, W.J., and Kinney, J.H., Viscoelastic properties of demineralized human dentin measured in water with atomic force microscope (AFM)-based indentation. *J. Biomed. Mater. Res.*, **15** (1998), 539–44.

[BAb] Balooch, G., Marshall, G.W., Marshall, S.J., Warren, O.L., Asif, S.A., and Balooch, M., Evaluation of a new modulus mapping technique to investigate microstructural features of human teeth. *J. Biomech.*, **37** (2004), 1223–32.

[BAc] Bargren, J.H., Andrew, C., Bassett, L., and Gjelsvik, A., Mechanical properties of hydrated cortical bone. *J. Biomech.*, **7** (1974), 239–45.

[BAd] Bayraktar, H.H. and Keaveny, T.M., Mechanisms of uniformity of yield strains for trabecular bone. *J. Biomech.*, **37** (2004), 1671–8.

[BEa] Behiri, J.C. and Bonfield, W., Fracture mechanics of bone—the effects of density, specimen thickness and crack velocity on longitudinal fracture. *J. Biomech.*, **17** (1984), 25–34.

[BOa] Bonfield, W. and Datta, P.K., Fracture toughness of compact bone. *J. Biomech.*, **9** (1976), 131–4.

[BOb] Bonfield, W. and Grynpas, M.D., Anisotropy of the Young's modulus of bone. *Nature*, **270** (1977), 453–4.

[BOc] Boskey, A., Bone mineral crystal size. *Osteoporos. Int.*, **14** (2003), 16–21.

[BOd] Boyde, A. and Jones, S.J., Scanning electron microscopy of bone: Instrument, specimen, and issues. *Microscopy Res. Tech.*, **33** (1998), 92–120.

[BOe] Bowen, R.L. and Rodriguez, M.S., Tensile strength and modulus of elasticity of tooth structure and several restorative materials. *J. Am. Dent. Assoc.*, **64** (1962), 378–87.

[BRa] Bromage, T.G., Goldman, H.M., McFarlin, S.C., Warshaw, J., Boyde, A., and Riggs, C.M., Circularly polarized light standards for investigations of collagen fiber orientation in bone. *Anat. Rec. B. New Anat.*, **274** (2003), 157–68.

[BRb] Brown, S.J., Pollintine, P., Powell, D.E., Davie, M.W.J., and Sharp, C.A., Regional differences in mechanical and material properties of femoral head cancellous bone in health and osteoarthritis. *Calcif. Tissue Int.*, **71** (2002), 227–234.

[BUa] Bumrerraj, S. and Katz, J.L., Scanning acoustic microscopy study of human cortical and trabecular bone. *Ann. Biomed. Eng.*, **29** (2001), 1034–42.

[BUb] Burr, D.B., Schaffler, M.B., and Frederickson, R.G., Composition of the cement line and its possible mechanical role as a local interface in human compact bone. *J. Biomech.*, **21** (1988) 939–45.

[CAa] Cagidiaco, M.C. and Ferrari, M., Organization of the matrix. In: Bonding to dentin. Livorno: O. Debatte and F. Ed. (1995), 11–26.

[CAb] Carter, D.R. and Hayes, W.C., The compressive behavior of bone as two-phase porous structure. *J. Bone Joint Surg.*, **59** (1977), 954–962.

[CAc] Carter, D.R. and Caler, W.E., Cycle-dependent and time-dependent bone fracture with repeated loading. *J. Biomech. Eng.*, **105** (1983), 166–70.

[CAd] Cassidy, J.J., Hiltner, A., and Baer, E., Hierarchical structure of the intervertebral disc. *Connect Tissue Res.*, **1** (1989), 75–88.

[CAe] Causa, F., Manto, L., Borzacchiello, A., De Santis, R., Netti, P.A., Ambrosio, L., and Nicolais, L., Spatial and structural dependence of mechanical properties of porcine intervertebral disc. *J. Mater. Sci. Mater. Med.*, **12** (2002), 1277–80.

[CHa] Charras, G.T., Lehenkari, P.P., and Horton, M.A., Atomic force microscopy can be used to mechanically stimulate osteoblasts and evaluate cellular strain distributions. *Ultramicroscopy.*, **86** (2001), 85–95.

[CHb] Choi, K., Kuhn, J.L., Ciarelli, M.J., and Goldstein, S.A., The elastic moduli of human subchondral, trabecular, and cortical bone tissue and the size-dependency of cortical bone modulus. *J. Biomech.*, **11** (1990), 1103–1113.

[CHc] Choi, K. and Goldstein, S.A., A comparison of the fatigue behavior of human trabecular and cortical bone tissue. *J. Biomech.*, **25** (1992), 1371–81.

[CIa] Ciarelli, T.E., Fyhrie, D.P., Schaffler, M.B., and Goldstein, S.A., Variations in three-dimensional cancellous bone architecture of the proximal femur in female hip fractures and in controls. *J. Bone Miner. Res.*, **15** (2000), 32–40.

[CLa] Claes, L.E., Wilke, H.J., and Kiefer, H., Osteonal structure better predicts tensile strength of healing bone than volume fraction. *J. Biomech.*, **28** (1995), 1377–90.

[COa] Courtney, A.C., Hayes, W.C., and Gibson, L.J., Age-related differences in post-yield damage in human cortical bone. Experiment and model. *J. Biomech.*, **29** (1996), 1463–71.

[COb] Cowin, S.C. and Turner, C.H., On the relationship between the orthotropic Young's moduli and fabric. *J. Biomech.*, **25** (1992), 1493–1494.

[COc] Cowin, S.C., Bone poroelasticity. *J. Biomech.*, **32** (1999), 217–38.

[COd] Cowin, S.C., The relationship between the elasticity tensor and the fabric tensor. *Mech. Mater.*, **4** (1985), 134–147.

[COe] Cowin, S.C., Wolff's law of trabecular architecture at remodeling equilibrium. *J. Biomech. Eng.*, **1** (1986), 83–8.

[CRa] Craig, R.G. and Peyton, F.A., Elastic and mechanical properties of human dentin. *J. Dent. Res.*, **37** (1958), 710–8.

[CRb] Craig, R.G. and Peyton, F.A., Thermal conductivity of teeth structures, dentin cements, and amalgam. *J. Dent. Res.* **40** (1961), 411–418.

[CUa] Cuppone, M., Seedhom, B.B., Berry, E., Ostell, A.E., The longitudinal Young's modulus of cortical bone in the midshaft of human femur and its correlation with CT scanning data. *Calcif. Tissue Int.*, **74** (2004), 302–9.

[CUb] Currey, J.D., Stress concentrations in bone. *Q J. Microsc. Sci.*, **103** (1962), 111–133.

[CUc] Currey, J., Sacrificial bonds heal bone. *Nature*, **414** (2001), 699.

[CUd] Currey, J.D. and Butler, G., The mechanical properties of bone tissue in children. *J. Bone Joint Surg. Am.*, **57** (1975), 810–4.

[DAa] Dabestani, M. and Bonfield, W., Elastic and anelastic microstrain measurement in human cortical bone. In: **Implant Materials in Biofunction**. de Putter, C., de Lange, G.L., de Groot, K., Lee, A.J.C. Eds. Elsevier Science, Amsterdam (1988), 435–440.

[DEa] De Santis, R., Mollica, F., Prisco, D., Rengo, S., Ambrosio, L., and Nicolais, L., A 3-D analysis of mechanically stressed dentin-adhesive-composite interfaces using X-ray micro-CT. *Biomaterials*, **26** (2005), 257–270.

[DEb] De Santis, R., Anderson, P., Tanner, K.E., Ambrosio, L., Nicolais L., Bonfield, W., and Davis, G.R., Bone fracture analysis on the short rod chevron-notch specimens using the X-ray computer micro-tomography. *J. Mat. Sci. Mat. Med.*, **11** (2000), 629–636.

[DEc] Deligiann, D.D., Missirlis, Y.F., Tanner, K.E., and Bonfield, W., Mechanical behavior of trabecular bone of the human femoral head in females. *J. Mater. Sci. Mat. Med.*, **2** (1991), 168–175.

[DEd] Deligiann, D.D., Maris, A., and Missirlis, Y.F., Stress relaxation behavior of trabecular bone specimens. *J. Biomech.*, **27** (1994), 1469–1476.

[DIa] Ding, M., Dalstra, M., Danielsen, C.C., Kabel, J., Hvid, I., and Linde, F., Age variations in the properties of human tibial trabecular bone. *J. Bone Joint Surg. Br.*, **6** (1997), 995–1002.

[DOa] Dowling, N.E., **Mechanical Behavior of Materials**. Prentice-Hall, Englewood Cliffs, NJ (1996).

[DUa] Duncanson, M.G., Jr. Korostoff, E., Compressive viscoelastic properties of human dentin: I. Stress-relaxation behavior. *J. Dent. Res.*, **54** (1975), 1207–12.

[ELa] El Mowafy, O.M. and Watts, D.C., Fracture toughness of human dentin. *J. Dent. Res.*, **65** (1986), 677–81.

[ERa] Erdemt, U., Instrument science and technology: Force and weight measurement, *J. Phys E: Sci. Instrum.*, **15** (1982), 857–872.

[EVa] Evans, F.G. and Vincentelli, R., Relation of collagen fibers orientation to some mechanical properties of human cortical bone. *J. Biomech.*, **2** (1969), 63–71.

[FAa] Fan, Z. and Rho, J.Y., Effects of viscoelasticity and time-dependent plasticity on nanoindentation measurements of human cortical bone. *J. Biomed. Mater. Res. A*, **67** (2003), 208–14.

[FAb] Fantner, G.E., Hassenkam, T., Kindt, J.H., Weaver, J.C., Birkedal, H., Pechenik, L., Cutroni, J.A., Cidade, G.A.G., Stucky, G.D., Morse, D.E., and Hansma, P.K., Sacrificial bonds and hidden length dissipate energy as mineralized fibrils separate during bone fracture. *Nature*, **4** (2005), 612–616.

[FOa] Fong, H., Sarikaya, M., White, S.N., and Snead, M.L., Nano-mechanical properties profiles across dentin-enamel junction of human incisor teeth. *Mater. Sci. Eng. C*, **7** (2000), 119–128.

[FOb] Forss, H., Seppa, L., and Lappalainen, R., In vitro abrasion resistance and hardness of glass-ionomer cements. *Dent. Mater.*, **7** (1991), 36–9.

[GAa] Galante, J., Rostoker, W., and Ray, R.D., Physical properties of trabecular bone. *Calcif Tissue Res.*, **5** (1970), 236–46.

[GAb] Garberoglio, R. and Brannstrom, M., Scanning electron microscopic investigation of human dentinal tubules. *Arch. Oral Biol.*, **21** (1976), 355–62.

[GIa] Giesen, E.B., Ding, M., and Dalstra, M., and van Eijden, T.M., Mechanical properties of cancellous bone in the human mandibular condyle are anisotropic. *J. Biomech.*, **34** (2001), 799–803.

[GIb] Gilmore, R.S. and Katz, J.L., Elastic properties of apatites, *J. Mat. Sci.*, **17** (1982), 1131–1141.

[GOa] Goldstein, S.A., Wilson, D.L., Sonstegard, D.A., and Matthews, L.S., The mechanical properties of human tibial trabecular bone as a function of metaphyseal location. *J. Biomech.*, **12** (1983), 965–969.

[GUa] Guo, X.E., Liang, L.C., and Goldstein, S.A., Micromechanics of osteonal cortical bone fracture. *J. Biomech. Eng.*, **120** (1998), 112–7.

[HAa] Habelitz, S., Marshall, G.W., Jr., Balooch, M., and Marshall, S.J., Nanoindentation and storage of teeth. *J. Biomech.*, **35** (2002), 995–8.

[HAb] Habelitz, S., Marshall, S.J., Marshall, G.W., Jr., and Balooch, M., Mechanical properties of human dental enamel on the nanometre scale. *Arch. Oral Biol.*, **46** (2001), 173–83.

[HAc] Hara, T., Takizawa, M., Sato, T., and Ide, Y., Mechanical properties of buccal compact bone of the mandibular ramus in human adults and children: Relationship of the elastic modulus to the direction of the osteon and the porosity rati. *Bull. Tokyo Dent. Coll.*, **39** (1998), 47–55.

[HAd] Hassan, R., Caputo, A.A., and Bunshah, R.F., Fracture toughness of human enamel. *J. Dent. Res.*, **60** (1981), 820–7.

[HEa] Hengsberger, S., Kulik, A., and Zysset, P., Nanoindentation discriminates the elastic properties of individual human bone lamellae under dry and physiological conditions. *Bone*, **30** (2002), 178–84.

[HOa] Hogan, H.A., Micromechanics modeling of Haversian cortical bone properties. *J. Biomech.*, **25** (1992), 549–56.

[HOb] Homminga, J., McCreadie, B.R., Ciarelli, T.E., Weinans, H., Goldstein, S.A., and Huiskes, R., Cancellous bone mechanical properties from normals and patients with hip fractures differ on the structure level, not on the bone hard tissue level. *Bone*, **30** (2002), 759–64.

[HVa] Hvid, I. and Hansen, S.L., Trabecular bone strength patterns at the proximal tibial epiphysis. *J. Orthop. Res.*, **4** (1985), 464–472.

[HUa] Huiskes, R. Ruimerman, R., van Lenthe, G.H., and Janssen, J.D., Effects of mechanical forces on maintenance and adaptation of form in trabecular bone. *Nature*, **405** (2000), 704–706.

[IMa] Imbeni, V., Nalla, R.K., Bosi, C., Kinney, J.H., and Ritchie, R.O., In vitro fracture toughness of human dentin. *J. Biomed. Mater. Res. A*, **66** (2003), 1–9.

[ITa] Ito, S., Saito, T., Tay, F.R., Carvalho, R.M., Yoshiyama, M., and Pashley, D.H., Water content and apparent stiffness of non-caries versus caries-affected human dentin. *J. Biomed. Mater. Res. B Appl. Biomater.*, **72** (2005), 109–16.

[IWa] Iwamoto, N. and Ruse, N.D., Fracture toughness of human dentin. *J. Biomed. Mater. Res. A*, **66** (2003), 507–12.

[JAa] Jantarat, J., Palamara, J.E., Lindner, C., and Messer, H.H., Time-dependent properties of human root dentin. *Dent. Mater.*, **18** (2002), 486–93.

[JAb] Jasiuk, I. and Ostoja-Starzewski, M., Modeling of bone at a single lamella level. *Biomech. Model Mechanobiol.*, **3** (2004), 67–74.

[JEa] Jepsen, K.J. and Davy, D.T., Comparison of damage accumulation measures in human cortical bone. *J. Biomech.*, **30** (1997), 891–4.

[KAa] Kabel, J., van Rietbergen, B., Odgaard, A., and Huiskes, R., Constitutive relationships of fabric, density, and elastic properties in cancellous bone architecture. *Bone*, **25** (1999), 481–486.

[KAa] Kafka, V. and Jirova, J., A structural mathematical model for the viscoelastic anisotropic behavior of trabecular bone. *Biorheology*, **20** (1983), 795–805.

[KAb] Katz, J.L. and Meunier, A., Material properties of single osteons and osteonic lamellae using high frequency scanning acoustic microscopy. In: **Bone Structure and Remodeling**. Odgaard, A., Weinas, H., Eds. Word Scientific, Amsterdam (1994), 157–165.

[KAc] Katz, J.L., Anisotropy of Young's modulus of bone. *Nature*, **283** (1980), 106–7.

[KEa] Keaveny, T.M. and Hayes, W.C., A 20-year perspective on the mechanical properties of trabecular bone. *J. Biomech. Eng.* **115** (1993), 534–42.

[KEb] Keaveny, T.M., Morgan, E.F., Niebur, G.L., and Yeh, O.C., Biomechanics of trabecular bone. *Annu. Rev. Biomed. Eng.*, **3** (2001), 307–333.

[KIa] Kinney, J.H., Balooch, M., Marshall, S.J., Marshall, G.W., Jr., Weihs, T.P., Hardness and Young's modulus of human peritubular and intertubular dentine. *Arch. Oral Biol.*, **41** (1996), 9–13.

[KIb] Kinney, J.H., Balooch, M., Marshall, S.J., Marshall, G.W., Jr., and Weihs, T.P., Atomic force microscope measurements of the hardness and elasticity of peritubular and intertubular human dentin. *J. Biomech. Eng.*, **118** (1996), 133–5.

[KIc] Kinney, J.H., Balooch, M., Marshall, G.W., and Marshall, S.J., A micromechanics model of the elastic properties of human dentine. *Arch. Oral Biol.*, **44** (1999), 813–22.

[KId] Kinney, J.H., Marshall, S.J., and Marshall, G.W., The mechanical properties of human dentin: A critical review and re-evaluation of the dental literature. *Crit. Rev. Oral Biol. Med.*, **14** (2003), 13–29.

[KIe] Kinney, J.H., Gladden, J.R., Marshall, G.W., Marshall, S.J., So, J.H., and Maynard, J.D., Resonant ultrasound spectroscopy measurements of the elastic constants of human dentin. *J. Biomech.*, **37** (2004), 437–41.

[KIf] Kishen, A., Ramamurty, U., and Asundi, A., Experimental studies on the nature of property gradients in the human dentine. *J. Biomed. Mater. Res.*, **51** (2000), 650–9.

[KOa] Konishi, N., Watanabe, L.G., Hilton, J.F., Marshall, G.W., Marshall, S.J., and Staninec, M., Dentin shear strength: Effect of distance from the pulp. *Dent. Mater.*, **18** (2002), 516–20.

[KOb] Kopperdahl, D.L. and Keaveny, T.M., Yield strain behavior of trabecular bone. *J. Biomech.*, **31** (1998), 601–608.

[KUa] Kuboky, Y. and Mechanic, G.L., Comparative molecular distribution of cross-link in bone and dentine collagen. Structure-function relationship. *Calcif. Tissue Int.*, **34** (1982), 306–308.

[LAa] Lakes, R.S., Nakamura, S., Behiri, J.C., and Bonfield, W., Fracture mechanics of bone with short cracks. *J. Biomech.*, **23** (1990), 967–75.

[LAb] Lang, H.P., Hegner, M., and Gerber, C., Cantilever array sensors. *Mater. Today*, **8** (2005), 30–36.

[LEa] Lenz, C. and Nackenhorst, U., A numerical approach to mechanosensation of bone tissue based on a micromechanical analysis of a single osteon. *PAMM*, **4** (2004), 342–343.

[LEb] Lertchirakarn, V., Palamara, J.E., and Messer, H.H., Anisotropy of tensile strength of root dentin. *J. Dent. Res.*, **80** (2001), 453–6.

[LIa] Liebschner, M.A. and Keller, T.S., Hydraulic strengthening affects the stiffness and strength of cortical bone. *Ann. Biomed. Eng.* **33** (2005), 26–38.

[LIb] Linde, F., Norgaard, P., Hvid, I., Odgaard, A., and Soballe, K., Mechanical properties of trabecular bone. Dependency on strain rate. *J. Biomech.*, **24** (1991), 803–809.

[LIc] Linde, F. and Sorensen, H.C., The effect of different storage methods on the mechanical properties of trabecular bone. *J. Biomech.*, **26** (1993), 1249–52.

[MAa] Majumdar, S., Kothari, M., Augat, P., Newitt, D.C., Link, T.M., Lin, J.C., Lang, T., Lu, Y., and Genant, H.K., High-resolution magnetic resonance imaging: Three-dimensional trabecular bone architecture and biomechanical properties. *Bone*, **22** (1998), 445–54.

[MAb] Marshall, G.W., Jr., Balooch, M., Gallagher, R.R., Gansky, S.A., and Marshall, S.J., Mechanical properties of the dentinoenamel junction: AFM studies of nanohardness, elastic modulus, and fracture. *J. Biomed. Mater. Res.*, **54** (2001), 87–95.

[MAc] Marshall, S.J., Balooch, M., Habelitz, S., Balooch, G., Gallagher, R., and Marshall, G.W., The dentin-enamel junction-a natural, multilevel interface. *J. Europ. Ceramic Soc.*, **23** (2003), 2897–2904

[MAd] Martin, R.B. and Burr, D.B., A hypothetical mechanism for the stimulation of osteonal remodeling by fatigue damage. *J. Biomech.*, **15** (1982), 137–9.

[MAe] Martin, B., Aging and strength of bone as a structural material. *Calcif. Tissue Int.*, **53 Suppl 1** (1993), S34–39.

[MCa] McElhaney, J.H., Dynamic response of bone and muscle tissue. *J. Appl. Physiol.*, **21** (1966), 1231–36.

[MEa] Mente, P.L. and Lewis, J.L., Experimental method for the measurement of the elastic modulus of trabecular bone tissue. *J. Orthop. Res.*, **7** (1989), 456–61.

[MEb] Meredith, N., Sherriff, M., Setchell, D.J., and Swanson, S.A., Measurement of the microhardness and Young's modulus of human enamel and dentine using an indentation technique. *Arch. Oral Biol.* **41** (1996), 539–45.

[MIa] Miguez, P.A., Pereira, P.N., Atsawasuwan, P., and Yamauchi, M., Collagen cross-linking and ultimate tensile strength in dentin. *J. Dent Res.*, **83** (2004), 807–10.

[MIb] Misch, C.E., Qu, Z., and Bidez, M.W., Mechanical properties of trabecular bone in the human mandible: implications for dental implant treatment planning and surgical placements. *J. Oral Maxillofac. Surg.*, **57** (1999), 700–706.

[MOa] Morgan, E.F. and Keaveny, T.M., Dependence of yield strain of human trabecular bone on anatomic site. *J. Biomech.*, **5** (2001), 569–77.

[MOb] Mosekilde, L., Mosekilde, L., and Danielsen, C.C., Biomechanical competence of vertebral trabecular bone in relation to ash density and age in normal individuals. *Bone*, **2** (1987), 79–85.

[NAa] Nalla, R.K., Kinney, J.H., and Ritchie, R.O., On the fracture of human dentin: Is it stress- or strain-controlled? *J. Biomed. Mater. Res.A*, **67** (2003), 484–95.

[NAb] Nalla, R.K., Imbeni, V., Kinney, J.H., Staninec, M., Marshall, S.J., and Ritchie, R.O., In vitro fatigue behavior of human dentin with implications for life prediction. *J. Biomed. Mater. Res.A* **66** (2003), 10–20.

[NAc] Nalla, R.K., Kinney, J.H., Marshall, S.J., and Ritchie, R.O., On the in vitro fatigue behavior of human dentin: Effect of mean stress. *J. Dent. Res.*, **83** (2004), 211–5.

[NAd] Natali, A.N., and Hart, R.T., Mechanics of hard tissues, in Integrated Biomaterials Science, R. Barbucci, Ed. Kluwer Academic and Plenum, New York (2002) 459–489.

[NIa] Nicholson, P.H., Muller, R., Lowet, G., Cheng, X.G., Hildebrand, T., Ruegsegger, P., van der Perre, G., Dequeker, J., and Boonen, S., Do quantitative ultrasound measurements reflect structure independently of density in human vertebral cancellous bone? *Bone*, **23** (1998), 425–31.

[NIb] Nicholson, P.H.F., Cheng, X.G., Lowet, G., Boonen, S., Davie, M.W.J., Dequeker, J., and Van der Perre, G., Structural and material mechanical properties of human vertebral cancellous bone. *Med. Eng. Phys.*, **19** (1997), 729–737.

[NIc] Nicolais, L., Mechanics of composites (particulate and fiber polymeric laminate properties). *Polym. Eng. Sci.*, **15** (1975), 137–149.

[NOa] Norman, T.L., Vashishth, D., and Burr, D.B., Mode I fracture toughness of human bone. In: **Advances in Bioengineering**, Vanderby, R., Ed. ASME, New York (1991), pp. 361–364.

[NOb] Norman, T.L., Vashishth, D., and Burr, D.B., Fracture toughness of human bone under tension. *J. Biomech.*, **28** (1995), 309–20.

[NOc] Norman, T.L., Nivargikar, S.V., and Burr, D.B., Resistance to crack growth in human cortical bone is greater in shear than in tension. *J. Biomech.*, **29** (1996), 1023–31.

[NOd] Norman, T.L. and Wang, Z., Microdamage of human cortical bone: Incidence and morphology in long bones. *Bone*, **20** (1997), 375–9.

[OKa] Okazaki, K., Nishimura, F., and Nomoto, S., Fracture toughness of human enamel. *Shika Zairyo Kikai*, **8** (1989), 382–7.

[OMa] O'Mahony, A.M., Williams, J.L., Katz, J.O., and Spencer, P., Anisotropic elastic properties of cancellous bone from human edentulous mandible. *Clin. Oral Impl. Res.*, **11** (2000), 415–421.

[OUa] Ouyang, J., Yang, G.T., Wu, W.Z., Zhu, Q.A., and Zhong, S.Z., Biomechanical characteristics of human trabecular bone. *Clin. Biomech.* **12** (1997), 522–524.

[PAa] Pashley, D.H., Agee, K.A., Wataha, J.C., Rueggeberg, F., Ceballos, L., Itou, K., Yoshiyama, M., Carvalho, R.M., and Tay, F.R., Viscoelastic properties of demineralized dentin matrix. *Dent. Mater.*, **19** (2003), 700–6.

[RAa] Rasmussen, S.T., Patchin, R.E., Scott, D.B., and Heuer, A.H., Fracture properties of human enamel and dentin. *J. Dent. Res.*, **55** (1976), 154–64.

[RAb] Raum, K., Jenderka, K.V., Klemenz, A., and Brandt, J., Multilayer analysis: Quantitative scanning acoustic microscopy for tissue characterization at a microscopic scale. *IEEE Trans. Ultras Ferroelectr. Freq. Contr.*, **50** (2003), 507–516.

[REa] Reilly, D.T., Burstein, A.H., and Frankel, V.H., The elastic modulus for bone. *J. Biomech.*, **7** (1974), 271–5.

[REb] Reilly, D.T. and Burstein, A.H., The elastic and ultimate properties of compact bone tissue. *J. Biomech.*, **8** (1975), 393–405.

[REc] Renson, C.E. and Braden, M., Experimental determination of the rigidity modulus, Poisson's ratio and elastic limit in shear of human dentine. *Arch. Oral Biol.*, **20** (1975), 43–7.

[RHa] Rho, J.Y., Ashman, R.B., and Turner, C.H., Young's modulus of trabecular and cortical bone material: Ultrasonic and microtensile measurements. *J. Biomech.*, **2** (1993), 111–119.

[RHb] Rho, J.Y., Kuhn-Spearing, L., and Zioupos, P., Mechanical properties and the hierarchical structure of bone. *Med. Eng. Phys.*, **2** (1998), 92–102.

[RHc] Rho, J.Y., Roy, M.E., 2nd, Tsui, T.Y., and Pharr, G.M., Elastic properties of microstructural components of human bone tissue as measured by nanoindentation. *J. Biomed. Mater. Res.*, **45** (1999), 48–54.

[RHd] Rho, J.Y., An ultrasonic method for measuring the elastic properties of human tibial cortical and cancellous bone. *Ultrasonics*, **8** (1996), 777–783.

[ROa] Rohl, L., Larsen, E., Linde, F., Odgaard, A., and Jorgensen, J., Tensile and compressive properties of cancellous bone. *J. Biomech.* **12** (1991), 1143–9.

[ROb] Roy, M.E., Rho, J.Y., Tsui, T.Y., Evans, N.D., and Pharr, G.M., Mechanical and morphological variation of the human lumbar vertebral cortical and trabecular bone. *J. Biomed. Mater. Res.*, **44** (1999), 191–7.

[RUa] Runkle, J.C. and Pugh, J., The micro-mechanics of cancellous bone. II. Determination of the elastic modulus of individual trabeculae by a buckling analysis. *Bull. Hosp. Joint Dis.*, **36** (1975), 2–10.

[SAa] Sano, H., Shono, T., Sonoda, H., Takatsu, T., Ciucchi, B., Carvalho, R., and Pashley, D.H., Relationship between surface area for adhesion and tensile bond strength-evaluation of a micro-tensile bond test. *Dent. Mater*, **10** (1994), 236–40.

[SAb] Sano, H., Ciucchi, B., Matthews, W.G., and Pashley, D.H., Tensile properties of mineralized and demineralized human and bovine dentin. *J. Dent. Res.*, **73** (1994), 1205–11.

[SCa] Schaffler, M.B., Choi, K., and Milgrom, C., Aging and matrix microdamage accumulation in human compact bone. *Bone*, **17** (1995), 521–25.

[SCb] Schoenfeld, C.M., Lautenschlager, E.P., and Meyer, P.R., Mechanical properties of human cancellous bone in the femoral head. *Med. Biol. Engng.*, **12** (1974), 313–317.

[SCc] Schwartz-Dabney, C.L., Dechow, P.C., Schwartz-Dabney, C.L., and Dechow, P.C., Variations in cortical material properties throughout the human dentate mandible. *Am. J. Phys. Anthropol.*, **120** (2003), 252–77.

[SEa] Sevostianov, I. and Kachanov, M., Impact of the porous microstructure on the overall elastic properties of the osteonal cortical bone. *J. Biomech.*, **33** (2000), 881–8.

[SIa] Silver, F.H., Seehra, G.P., Freeman, J.W., and DeVore, D., Viscoelastic properties of young and old human dermis: A proposed molecular mechanism for elastic energy storage in collagen and elastin. *J. Appl. Pol. Sci.*, **79** (2001), 134–142.

[SIb] Simkin, A. and Robin, G., Fracture formation in differing collagen fiber pattern of compact bone. *J. Biomech.*, **7** (1974), 183–8.

[SKa] Skovoroda, A.R., Emelianov, S.Y., and O'Donnell, M., Tissue elasticity reconstruction based on ultrasonic displacement and strain images, *IEEE Trans. Ultrason. Ferroelectr. Freq. Contr.*, **42** (1995), 747–745.

[STa] Staninec, M., Marshall, G.W., Hilton, J.F., Pashley, D.H., Gansky, S.A., Marshall, S.J., and Kinney, J.H., Ultimate tensile strength of dentin: Evidence for a damage mechanics approach to dentin failure. *J. Biomed. Mater. Res.*, **63** (2002), 342–5.

[TAa] Tam, L.E. and Yim, D., Effect of dentine depth on the fracture toughness of dentine-composite adhesive interfaces. *J. Dent.*, **25** (1997), 339–46.

[TEa] Tesch, W., Eidelman, N., Roschger, P., Goldenberg, F., Klaushofer, K., and Fratzl, P., Graded microstructure and mechanical properties of human crown dentin. *Calcif Tissue Int.*, **69** (2001), 147–57.

[THa] Thompson, J.B., Kindt, J.H., Drake, B., Hansma, H.G., Morse, D.E., and Hansma, P.K., Bone indentation recovery time correlates with bond reforming time. *Nature*, **414** (2001), 773–776.

[TUa] Turner, C.H., Rho, J., Takano, Y., Tsui, T.Y., and Pharr, G.M., The elastic properties of trabecular and cortical bone tissues are similar: results from two microscopic measurement techniques. *J. Biomech.*, **32** (1999), 437–41.

[TYa] Tyldesley, W.R., The mechanical properties of human enamel and dentine. *Briti. Dent. J.*, **106** (1959), 269–278.

[ULa] Ulrich, D., van Rietbergen, B., Weinans, H., and Ruegsegger, P., Finite element analysis of trabecular bone structure: A comparison of image-based meshing techniques. *J. Biomech.*, **31** (1998), 1187–92.

[VAa] Van Lenthe, G.H. and Huiskes, R., How morphology predicts mechanical properties of trabecular structures depends on intra-specimen trabecular thickness variations. *J. Biomech.*, **9** (2002), 1191–1197.

[VAb] Van Meerbeek, B., Willems, G., Celis, J.P., Roos, J.R., Braem, M., Lambrechts, P., and Vanherle, G., Assessment by nano-indentation of the hardness and elasticity of the resin-dentin bonding area. *J. Dent. Res.*, **72** (1993), 1434–42.

[VAc] Van Rietbergen, B., Huiskes, R., Eckstein, F., and Ruegsegger, P., Trabecular bone tissue strains in the healthy and osteoporotic human femur. *J. Bone Miner. Res.*, **18** (2003), 1781–8.

[VAd] Vashishth, D., Behiri, J.C., and Bonfield, W., Crack growth resistance in cortical bone: Concept of microcrack toughening. *J. Biomech.*, **30** (1997), 763–9.

[VEa] Veis, A., Dentin. In: **Extracellular Matrix. Tissue Function**, Vol. 1. Comper WD, The Netherlands (1996), 41–75.

[WAa] Watanabe, L.G., Marshall, G.W., Jr., and Marshall, S.J., Dentin shear strength: effects of tubule orientation and intratooth location. *Dent. Mater.*, **12** (1996), 109–15.

[WAb] Watts, D.C., el Mowafy, O.M., and Grant, A.A., Temperature-dependence of compressive properties of human dentin. *J. Dent. Res.* **66** (1987), 29–32.

[WEa] Weiner, S. and Wagner, H.D., The material bone: Structure-mechanical function relations. *Ann. Rev. Mater. Sci.* **28** (1998), 271–298.

[WEb] Weyland, M. and Midgley, P.A., Electron tomography. *Mater. Today*, **7** (2004), 32–40.

[WIb] Willems, G., Lambrechts, P., Braem, M., Celis, J.P., and Vanherle, G., A classification of dental composites according to their morphological and mechanical characteristics. *Dent. Mater.*, **8** (1992), 310–9.

[WIc] Willems, G., Celis, J.P., Lambrechts, P., Braem, M., and Vanherle, G., Hardness and Young's modulus determined by nanoindentation technique of filler particles of dental restorative materials compared with human enamel. *J. Biomed. Mater. Res.*, **27** (1993), 747–55.

[WOa] Wolff, J., **Das Gesetz der Transformation der Knochen**. Published with support from the Royal Academy of Sciences in Berlin. A. Hirschwald, ed. Berlin, 1892. English trans. by P. Maquet and R. Furlong. **The Law of Bone Remodeling**. Belin, Springer-Verlag, Heidelberg (1986).

[XUa] Xu, H.H., Smith, D.T., Jahanmir, S., Romberg, E., Kelly, J.R., Thompson, V.P., and Rekow, E.D., Indentation damage and mechanical properties of human enamel and dentin. *J. Dent. Res.*, **77** (1998), 472–80.

[XUb] Xu, J., Rho, J.Y., Mishra, S.R., and Fan, Z., Atomic force microscopy and nanoindentation characterization of human lamellar bone prepared by microtome sectioning and mechanical polishing technique. *J. Biomed. Mater. Res. A*, **67** (2003), 719–26.

[YAa] Yamamoto, E., Crawford, P.R., Chan, D.D., and Keaveny, T.M., Development of residual strains in human vertebral trabecular bone after prolonged static and cyclic loading at low load levels. *J. Biomech.* **39**(10) (2006), 1812–8.

[YAb] Yamashita, J., Furman, B.R., Rawls, H.R., Wang, X., and Agrawal, C.M., The use of dynamic mechanical analysis to assess the viscoelastic properties of human cortical bone. *J. Biomed. Mater. Res.* **58** (2001), 47–53.

[YOa] You, L.D., Weinbaum, S., Cowin, S.C., and Schaffler, M.B., Ultrastructure of the osteocyte process and its pericellular matrix. *Anat. Rec. A Discov. Mol. Cell Evol. Biol.*, **278** (2004), 505–13.

[YUa] Yu, Z. and Boseck, S., Scanning acoustic microscopy and its applications to material characterization. *Rev. Modern Phys.*, **67** (1995), 863–891.

[ZHa] Zhang, N. and Grimm, M.J., Measurement of elastic moduli of individual trabeculae of vertebtrae using scanning acoustic microscopy. *2001 Bioengineering Conference ASME*. Snowbird, Utah. **50** (2001), 283–284.

[ZIa] Zilch, H., Rohlmann, A., Bergmann, G., and Kolbel, R., Material properties of femoral cancellous bone in axial loading. Part II: Time dependent properties. *Arch. Orthop. Trauma Surg.*, **97** (1980), 257–62.

[ZIb] Zioupos, P., Wang, X.T., and Currey, J.D., Experimental and theoretical quantification of the development of damage in fatigue tests of bone and antler. *J. Biomech.*, **29** (1996), 989–1002.

[ZIc] Zioupos, P., X, T.W., and Currey, J.D., The accumulation of fatigue microdamage in human cortical bone of two different ages in vitro. *Clin. Biomech.*, **11** (1996), 365–375.

[ZId] Zioupos, P., Currey, J.D., and Hamer, A.J., The role of collagen in the declining mechanical properties of aging human cortical bone. *J. Biomed. Mater. Res.*, **45** (1999), 108–16.

[ZYa] Zysset, P.K., Guo, X.E., Hoffler, C.E., Moore, K.E., and Goldstein, S.A., Elastic modulus and hardness of cortical and trabecular bone lamellae measured by nanoindentation in the human femur. *J. Biomech.*, **32** (1999), 1005–12.